



SHIRSHOV INSTITUTE OF OCEANOLOGY

CRUISE REPORT No. 44

RV *AKADEMIK IOFFE* CRUISE 30 June - 19 July 2014

**North Atlantic Repeat Hydrography of
WOCE section along 59.5 N**

Principal Scientists **A. Sokov¹ & S. Gladyshev¹**

2015

Shirshov Institute of Oceanology
36 Nakhimovskii prospect
Moscow 117997 RUSSIA
Tel: +7(495) 719 0255 Fax:
+7(499) 124 6342 Email:

sgladyshev@ocean.ru

¹Shirshov Institute of
Oceanology

DOCUMENT DATA SHEET

AUTHOR GLADYSHEV, S	PUBLICATION DATE 2015
TITLE RV <i>Akademik Ioffe</i> Cruise 44 , 30 June - 19 July 2014.	
REFERENCE Shirshov Institute of Oceanology, Akademik Ioffe Cruise Report, No. 44, 64pp. tables & figs.	

ABSTRACT

RV *Akademik Ioffe* Cruise 44 was a contribution to the Russian CLIVAR and WORLD OCEAN Research Programmes. CTD section was designed to enable the ocean circulation in the Subpolar gyre of the North Atlantic to be mapped and in particular the course of the North Atlantic, Irminger and East Greenland Currents within the region to be determined. The main goal is to continue annual monitoring of the North Atlantic large-scale circulation and climate changes in the North Atlantic.

11 stations (3220-3230) were made at the Greenland shelf and continental slope to determine the shelf East Greenland Current.

KEYWORDS

CRUISE 44 2014, AKADEMIK IOFFE, CLIVAR, TRANSATLANTIC SECTION, EAST GREENLAND CURRENT, IRMINGER BASIN, NORTH ATLANTIC SUBPOLAR GYRE, CLIVAR, CTD OBSERVATIONS, LADCP, VMADCP

ISSUING ORGANISATION

Shirshov Institute of Oceanology
36 Nakhimovskii prospect
Moscow 117997 RUSSIA

Director: Academician Robert Nigmatulin

Copies of this report are available from: **Department of Marine Operations**, Tel: +7(495)7190255 Fax: +7(499)124 6342

Email: sgladyshev@ocean.ru

Contents

Scientific Personnel

1. Cruise Narrative

1.1 Cruise Details

1.2 Cruise Summary

1.2.1 Cruise Track and Stations

1.2.2 Equipment

1.2.3 Sampling

1.2.4 Number of Stations Occupied

1.3 Scientific Objectives

1.4 Narrative

1.4.1 Introduction

1.4.2 Deep convection in the Irminger Sea

1.4.3 Reverse of the deep water freshening

1.4.4 Deep ocean salinity changes and NAO

1.4.5 Deep ocean salinity changes and climate change

1.4.6 Decadal variability of the DWBC at Cape Farewell

1.4.7 Mean state of the full depth circulation in 2000s

1.4.8 Cascading of dense shelf water in the Irminger Sea

1.5 Preliminary Results

1.6 Major Problems and Goals not achieved

2. Continuous Measurements (on station and underway)

2.1 Navigation

2.2 Meteorological Measurements

2.3 Thermosalinograph

2.4 Echosounding

2.5 Vessel Mounted Acoustic Doppler Current Profiler (OS 38 kHz)

3. On-Station Measurements

3.1 CTD

3.1.1 Equipment

3.1.2 Data processing and calibration

3.1.3 Final post-cruise CTD calibration

3.1.4 SBE 43 dissolved oxygen sensor calibration using Winkler Titration

3.2 Oxygen Bottle Samples

3.3 Nutrient Bottle Samples

3.4 Lowered Acoustic Doppler Current Profiler (LADCP)

3.4.1 LADCP Processing for Current Profile

3.5 Carbonate system measurements

3.5.1. Measured parameters

3.5.2. Sampling procedures

3.5.3 Stations and parameters sampled

3.6 Phytoplankton production in the North Atlantic

4. Cruise Logistics

5. Acknowledgements

Tables

Figures

Scientific Personnel

SOKOV, A	Principal Scientist	Shirshov
GLADYSHEV, S.	Co-Principal Scientist	Shirshov
PYATAKOV, V.	Chief of CTD group	Shirshov Atlantic Branch
GLADYSHEV, S.	CTD, LADCP, Sampling	Shirshov
ZAPOTYL'KO, V.	CTD, LADCP	Shirshov
AGARKOV, A.	CTD, LADCP, Sampling	Shirshov
KULESHOV, A.	Winch	Shirshov Atlantic Branch
LUKASHIN, S.	Winch, Sampling	Shirshov Atlantic Branch
MARKINA, M	CTD, LADCP, Sampling	Shirshov
DUKHOVA, L.	Chief of Chemistry group	Shirshov
SEREBRENIKOVA, E.	Oxygen	Shirshov
KOLOKOLOVA, A.	Oxygen	Shirshov
MEL'NIKOVA Z.	Nutrients	Shirshov
DEMIDOV, A.	Primary Production, Chl	Shirshov
MOSHAROV, S.	Primary Production, Chl	Shirshov
GAGARIN, V	Primary Production, Chl	Shirshov
KRINITSKII, M.	Meteo	Shirshov
GAVRIKOV, A.	Meteo	Shirshov
SANTANA, M.	CO ₂	University of Las Palmas
GONZÁLEZ, M.	CO ₂	University of Las Palmas
GONZÁLEZ, D.	CO ₂	University of Las Palmas
GONZÁLEZ, K.	CO ₂	University of Las Palmas

1. CRUISE NARRATIVE

1.1 Cruise Details

Expedition Designation: R/V *Akademik Ioffe* Cruise 44, RUSSIA CLIVAR

Principal Scientists: Dr Alexey Sokov and Dr. Sergey V. Gladyshev (Shirshov).

Ship: RV *Akademik Ioffe*.

Ports of Call: Gdansk (Poland) to Iqaluit (Canada).

Cruise Dates: 30th June to 19th July 2014.

1.2 Cruise Summary

1.2.1 Cruise Track and Stations

The cruise track with station positions is shown in **Fig. 1**. Only small volume samples were taken, details are listed in **Table 1**.

1.2.2. Equipment

The principal instruments used during the cruise were a SBE 9P-743 CTD with dual temperature and conductivity sensors (SBE 3 SN 03P5677, SBE 4 SN 042827, SBE 3 SN 03P4401, SBE 4 SN 042925), oxygen sensor (SBE 43, SN 430699), turbidity sensor (SeaPoint Turbidity, SN 10218 STM), Benthos altimeter model PSA-900D, LADCP WHS-300 kHz down-looking (S/N 6393), LADCP WHS-300 kHz up-looking (S/N 14151). These were mounted together with a multisampler Carousel SBE 32 equipped with 22 5-litre Niskin bottles. Upon recovery each bottle was sampled in turn for dissolved oxygen, nutrients, salinity. All sampling was done on deck. Currents were measured using vessel mounted ADCP (VMADCP) TRDI OS38 kHz (S/N 1185) installed at the central point of the ship hall.

Navigation information was provided by a Trimble SPSx50/SPSx51 - Modular GPS receiver and every second was recorded on the PC. Additional measurements were made with an ELAC 12 kHz, Aanderaa meteorological package.

1.2.3 Sampling

Nominal depths sampled were: bottom, 3100, 3000, 2750, 2500, 2250, 2000, 1750, 1500, 1250, 1100, 1000, 900, 800, 700, 600, 500, 400, 300, 200, 150, 100, 50, 30, 20, 10 m. On deep casts fewer shallow and intermediate bottles were fired. The actual bottle depths are shown in **Fig. 2**.

1.2.4 Number of Stations Occupied

76 stations (77 casts) were occupied during the cruise along transatlantic section along 59.5 N (**Fig. 1**).

1.3 Scientific Objectives

The cruise objectives were to:

1. To complete a CTD section from the Great Britain to Greenland.
2. To survey the North Atlantic Subpolar Gyre with high-resolution CTD and LADCP/VMADCP data to determine the circulation and meridional fluxes.

1.4 Narrative

1.4.1 Introduction

The Meridional overturning circulation (MOC) in the North Atlantic is one of the main drivers of the widely known global oceanic “conveyor belt” – an important element of the Earth’s climate system [e.g., van Aken, 2007]. Warm upper-ocean waters transported northward by the North Atlantic Current release heat to the atmosphere, gain density due to cooling and eventually sink in the subpolar North Atlantic and adjacent Arctic seas thereby generating the return southward flow of colder waters at depths (**Fig. 3**) [Dickson and Brown, 1994; Koltermann et al., 1999]. Temporal variability of the large-scale circulation and associated heat transport in the subpolar North Atlantic is one of the principal factors behind the high-latitude climate anomalies in the Northern Hemisphere.

Progress in understanding the causes of the ongoing climate change and forecasting climate variability in the Arctic and over European part of Russia for the next decades require reliable observation-based estimates of the variability of the North Atlantic circulation and the Atlantic–Arctic heat and freshwater fluxes, as well as elucidation of the underlying mechanisms.

In a number of recent studies, radical changes in the thermohaline regime and large-scale circulation in the Atlantic Ocean have been suggested to occur under global warming. For instance, the long-term freshening of the subpolar North Atlantic deep waters since the mid-1960s [Dickson et al., 2002] has been (cautiously) attributed to climate change-related factors [Curry et al., 2003; Hansen et al., 2004]. Hypothetically, under global warming, an increased evaporation in the tropics and increased precipitation at high latitudes, coupled with an intensified melting of Arctic ice, lead to the upper-ocean freshening in the regions of deep water formation and, hence, to the deep water freshening in the Atlantic Ocean. At the same time, milder winters along with the upper-ocean freshening lead to a decrease in the deep water production rates, which results in slowing of the Atlantic Meridional Overturning Circulation [e.g., Hansen et al., 2004; Bryden et al., 2005].

To better understand the past and present changes in the ocean-atmosphere dynamical system, as well as their causes and consequences, data on the full-depth oceanic variability are needed. An indispensable effective tool for assessing the large-scale circulation and thermohaline changes in the deep ocean and investigating mechanisms governing these changes are repeated full-depth transoceanic observations.

Since 1997, the P.P. Shirshov Institute of Oceanology has carried out the long-term monitoring of the North Atlantic circulation and water mass properties in the 59.5°N hydrographic section between Cape Farewell (Greenland) and Scotland (**Fig. 3**). Since 2002, the section has been repeated yearly on board the Russian research vessels, providing high precision data on temperature, salinity, oxygen and nutrients concentrations, and current velocities in the entire water column – “from shore to shore”, from the sea surface to the bottom. In 2011, in addition to annual repeat measurements at 59.5°N, the P.P. Shirshov Institute of Oceanology started full-depth repeat observations of the oceanic exchange between the Atlantic and Arctic oceans through the straits between Greenland, Iceland, Faeroe and Shetland Islands (**Fig. 3**). The full-depth observations – of the same oceanic quantities as at 59.5°N – are performed in the straits from research vessels twice a year, in summer and fall. Based on the unique data set thus collected, a number of fundamental findings have already been achieved. Below, we briefly summarize the main subjects and results of our research.

The 59.5°N transatlantic section (**Fig. 3**) was designed for monitoring the large-scale circulation and thermohaline / chemical properties of oceanic waters at the northern periphery of

the NA – the region where the warm upper-ocean waters are transformed by deep convection and mixing into the colder intermediate and deep waters – the Labrador Sea Water (LSW), Iceland Scotland Overflow Water (ISOW) and Denmark Strait Overflow Water (DSOW) (**Fig. 3**) – transported southward in the lower limb of the Atlantic MOC. Hydrographic data collected at 59.5°N along with those obtained within the framework of the kindred projects, primarily the French OVIDE (<http://www.ifremer.fr/lpo/ovide>), and historical data sets have been used for studying the dense water production [Falina et al., 2007; Falina et al., 2012], decadal temperature and salinity changes in the intermediate–deep water column [Sarafanov et al., 2007; Sarafanov et al., 2008; Sarafanov et al., 2010b], causes of these changes [Sarafanov, 2009; Sarafanov et al., 2010b], the mean state [Sarafanov et al., 2012] and long-term variability of the large-scale circulation in the region [Sarafanov et al., 2009; Sarafanov et al., 2010a; Våge et al., 2011].

1.4.2 Deep convection in the Irminger Sea

The oxygen data collected in 1997 in the northern North Atlantic in several sections ending nearby the southern tip of Greenland provided the observation-based support for the hypothesis [Pickart et al., 2003] that winter convection in the Irminger Sea may penetrate deep into the LSW layer (1000 – 2000 m) thus causing local renewal of this water mass. A separate lateral maximum of oxygen concentrations in the deep LSW layer was detected east of Cape Farewell (59.5°N, 36–40°W): the concentrations increased (by ~0.1 ml/l) from the Labrador Sea eastern edge toward the Irminger Sea (**Fig. 4**) rather than the reverse, as would be expected if LSW observed in the Irminger Sea interior in 1997 were solely of advective origin [Falina et al., 2007].

1.4.3. Reversal of the deep-water freshening

The LSW and Nordic Seas overflow-derived deep waters, ISOW and DSOW, freshened in the northern North Atlantic during the last three–four decades of the 20th century [Dickson et al., 2002]. Between the 1960s and 1990s, the water column in the region freshened on average by about 0.03 [Curry et al., 2003].

The long-term freshening reversed in the mid-1990s [Sarafanov et al., 2007; Sarafanov et al., 2008; Sarafanov et al., 2010b]. The salinification (and warming) of the intermediate and deep waters since the mid-1990s (**Fig. 5**) was much more intense than the preceding freshening. Over

nearly a decade (1997–2006), temperature / salinity in the intermediate–deep water column ($\sigma_0 \geq 27.45$, depths > 500 – 1000 m) at 59.5°N increased by $\sim 0.3^\circ\text{C} / 0.03$ – 0.04 [Sarafanov et al., 2008].

In the Irminger Sea, the long-term freshening in the deep water column ($\sigma_0 > 27.80$, depths $> \sim 2000$ m) reversed in the early 2000s [Sarafanov et al., 2010b]. The observed freshening reversal was a lagged consequence of the persistent ISOW salinification that occurred upstream, in the Iceland Basin, after 1996 due to salinification of the northeast Atlantic waters entrained into the overflow. It was demonstrated [Sarafanov et al., 2010b] that the entrainment salinity increase was associated with the North Atlantic Oscillation (NAO)-induced weakening and contraction of the Subpolar Gyre and corresponding northwestward advance of subtropical waters that followed the NAO decline in the mid-1990s and continued through the mid-2000s. Remarkably, the deep water freshening reversal was not related to changes in the overflow water salinity.

1.4.4. Deep-ocean salinity changes and the NAO

Close relationship between the thermohaline properties of the northern North Atlantic intermediate and deep waters and the winter NAO index on a decadal time scale ($r^2 \approx 0.65$, 1950s–2000s, **Fig. 6b** and **6c**) was revealed [Sarafanov, 2009] from the observation-based salinity time series for LSW in the Labrador Sea [Yashayaev, 2007] and ISOW in the Iceland basin [Boessenkool et al., 2007; Sarafanov et al., 2007]. Persistent NAO decline (amplification) leads to warming and salinification (cooling and freshening) in the intermediate–deep water column.

An explanation for the close link between the NAO and the coherent decadal changes in the intermediate and deep water properties in the region was proposed [Sarafanov, 2009]. The two factors dominate this link (**Fig. 6d**): (i) intensity of convection in the Labrador Sea controlling injection of relatively cold fresh waters into the intermediate layer and (ii) zonal extent of the Subpolar Gyre that regulates the relative contributions of cold fresh subpolar waters and warm saline subtropical waters to the entrainment into the Norwegian Sea overflow south of the Iceland–Scotland Ridge and to the Atlantic inflow to the Nordic Seas. These factors act in

phase leading to the observed coherent thermohaline changes in the intermediate–deep water column.

Due to weakening of the surface forcing associated with the NAO transition into neutral to low phase (1950s to mid-1960s, mid-1990s to mid-2000s), convection in the Labrador Sea weakens diminishing cold fresh water penetration into the intermediate layer. This results in warming and salinification at the intermediate depths in the Subpolar Gyre. Concurrently, the Subpolar Gyre contracts allowing northward advance of warm saline upper-ocean and intermediate subtropical waters in the northeastern North Atlantic. Northward progression of subtropical waters increases temperature and salinity at the upper intermediate levels and, correspondingly, increases temperature and salinity of the northeast Atlantic waters entrained into the Iceland–Scotland overflow along its pathway to the deep Iceland basin. As a result, temperature and salinity at the deep levels increase. The contrary changes – intensification of deep convection in the Labrador Sea and expansion of the Subpolar Gyre – caused by amplifying surface forcing (mid-1960s to mid-1990s) lead to cooling and freshening at the intermediate–deep levels. Additionally, under high-NAO conditions, deep convection may occur in the Irminger Sea potentially contributing to cooling and freshening at the intermediate (LSW) levels. The two regimes of convection and large-scale circulation corresponding to stronger (early 1990s) and weaker (mid-1960s, mid-2000s) NAO-related atmospheric forcing are schematically visualized in **Fig. 7**.

1.4.5 Deep-ocean salinity changes and climate change

There are increasing concerns that in the warmer climate, the MOC may substantially decline due to a decrease in the convective activity in the northern North Atlantic and Nordic Seas [e.g., [Meehl et al., 2007](#)]. The long-term freshening in the Nordic Seas and freshening of the northern North Atlantic deep waters in the 1960s–1990s have been considered as a likely indicator or precursor of the dramatic change in the MOC [e.g., [Hansen et al., 2004](#)]. The freshening has been attributed to a combination of factors potentially associated with the global warming: the increasing ice melt and net precipitation at high latitudes [e.g., [Curry et al., 2003](#)]. A probable causality between the climate change and the decreasing North Atlantic deep water salinity has supported the concerns and unfavorable predictions, thus ‘warming up’ the reasonable scientific debate on climate change and overblown speculations in media.

Despite the long-term increase in freshwater input to the Arctic, freshening in the northern North Atlantic had reversed in the mid-1990s, as we demonstrated above. This reversal forces us to revise the hypotheses on the mechanisms behind the deep-water thermohaline anomalies. It seems doubtful that the persistent global temperature growth may lead to the opposite decadal trends (positive-then-negative-then-positive, **Fig. 6**) in the deep water salinity.

Our results [[Sarafanov et al., 2008](#); [Sarafanov, 2009](#); [Sarafanov et al., 2010b](#)] suggest that natural atmospheric variability over the North Atlantic plays the major role in the deep-water thermohaline variability on a decadal time scale. There are no reasons to associate the deep-water freshening in the 1960s–1990s with climate change, unless the 3-decade-long surface forcing amplification is evidently shown to be a consequence of the latter. Having said that, the net 1950s–2000s trends in the water mass salinities are negative implying that the global factors (e.g., probable intensification of hydrological cycle [[Curry et al., 2003](#)]) may act on longer time scales.

1.4.6 Decadal variability of the Deep Western Boundary Current at Cape Farewell

Recent decadal changes in the Deep Western Boundary Current (DWBC) transport southeast of Cape Farewell were assessed from hydrographic data (1991–2007, **Fig. 7a**), direct velocity measurements (2002–2006) and satellite altimetry (1992–2007). Following the approach used in earlier studies [e.g., [Bacon, 1998](#)], we first determined that the DWBC ($\sigma_0 > 27.80$) baroclinic transport (T_{BC}) referenced to 1000 m depth increased by ~ 2 Sv between the mid-1990s (1994–1997) and 2000s (2000–2007) (**Fig. 8b**) [[Sarafanov et al., 2009](#)]. In the next step, we quantified velocity changes at the reference level (1000 m) by combining estimates of the hydrography-derived velocity changes in the water column and the altimetry-derived velocity changes at the sea surface [see [Sarafanov et al., 2010a](#)]. The inferred increase in the southward velocity at 1000 m above the DWBC in 1994–2007 indicates that the increase in the DWBC absolute transport was larger but very close to the 2-Sv increase in the DWBC T_{BC} . This result along with the observed coherence of the DWBC absolute and baroclinic transport changes between individual observations [[Sarafanov et al., 2010a](#)] imply that the DWBC absolute transport variability in the region is well represented by its baroclinic component on decadal and shorter time scales.

The historical record of the DWBC T_{BC} (1955–2007, **Fig. 8c**) updated after Bacon [1998] shows distinct decadal variability (± 2 – 2.5 Sv) with the transport minima in the 1950s and mid-1990s, maximum in the early 1980s and moderate-to-high transport in the 2000s. The DWBC T_{BC} decadal variability is consistent with the general pattern of the recent decadal hydrographic and circulation changes in the northern North Atlantic. The DWBC T_{BC} anomalies negatively correlate ($R = -0.80$, 1955–2007) with thickness anomalies of the Labrador Sea Water (LSW) at its origin implying a close link between the DWBC transport southeast of Cape Farewell and the LSW production in the Labrador Sea (**Fig. 8d**). During the recent three decades (late 1970s – late 2000s), the DWBC T_{BC} changes were also in-phase with changes in the strength and zonal extent of the Subpolar Gyre [see Sarafanov et al., 2010a]. In particular, the Gyre weakening at shallow levels in the mid-1990s – mid-2000s was accompanied by the DWBC strengthening in the Irminger Sea [Sarafanov et al., 2009; Sarafanov et al., 2010a; Våge et al., 2011]. The results imply that the decadal changes in the (i) LSW production, (ii) SPG strength and (iii) DWBC transport in the Irminger Sea are linked, representing a complex coherent oceanic response to the decadal variability of the surface forcing.

1.4.7 Mean state of the full-depth circulation in the 2000s

A mean state of the full-depth summer circulation in the Atlantic Ocean in the region in between Cape Farewell (Greenland), Scotland and the Greenland-Scotland Ridge (see **Fig. 3**) was assessed by combining 2002–2008 yearly hydrographic measurements at 59.5°N , mean dynamic topography, satellite altimetry data and available estimates of the Atlantic–Nordic Seas exchange [see Sarafanov et al., 2012]. The mean absolute transports by the upper-ocean, mid-depth and deep currents and the MOC ($\text{MOC}_{\sigma} = 16.5 \pm 2.2$ Sv, at $\sigma_0 = 27.55$) at 59.5°N were quantified in the density space. Inter-basin and diapycnal volume fluxes in between the 59.5°N section and the Greenland-Scotland Ridge were then estimated from a box model.

The estimated meridional and diapycnal volume fluxes contributing to the MOC are schematically visualized in **Fig. 9**. The dominant components of the meridional exchange across 59.5°N are the North Atlantic Current (NAC, 15.5 ± 0.8 Sv, $\sigma_0 < 27.55$) east of the Reykjanes Ridge, the northward Irminger Current (IC, 12.0 ± 3.0 Sv) and southward Western Boundary Current (WBC, 32.1 ± 5.9 Sv) in the Irminger Sea and the deep water export from the northern Iceland Basin (3.7 ± 0.8 Sv, $\sigma_0 > 27.80$). About 60% (12.7 ± 1.4 Sv) of waters carried in the MOC_{σ}

upper limb ($\sigma_0 < 27.55$) by the NAC/IC across 59.5°N (21.1 ± 1.0 Sv) recirculates westwards south of the Greenland-Scotland Ridge and feeds the WBC. 80% (10.2 ± 1.7 Sv) of the recirculating NAC/IC-derived upper-ocean waters gains density of $\sigma_0 > 27.55$ and contributes to the MOC σ lower limb. Accordingly, the contribution of light-to-dense water conversion south of the Greenland-Scotland Ridge (~ 10 Sv) to the MOC σ lower limb at 59.5°N is one and a half times larger than the contribution of dense water production in the Nordic Seas (~ 6 Sv).

1.4.8 Cascading of dense shelf waters in the Irminger Sea

Based on the hydrographic data collected at 59.5°N , 64.3°N and $65\text{--}66^\circ\text{N}$ in the western Irminger Sea in the 1990s – 2000s, an observational evidence for the deep-reaching cascading of dense shelf waters south of the Denmark Strait was found [Falina et al., 2012]. The data collected in the northwestern Irminger Sea ($65\text{--}66^\circ\text{N}$) indicate that the East Greenland Current ~ 200 km south of the Denmark Strait occasionally carries shelf waters as dense as the overflow-derived deep waters transported by the DWBC ($\sigma_0 > 27.80$). Hydrographic traces of cascading of dense shelf waters down the East Greenland slope were found from repeat measurements at 64.3°N , where the densest fresh plumes were observed within the DWBC ($\sigma_0 > 27.80$) (Fig. 10). Using the data collected at 59.5°N , we showed that the fresh ‘signals’ originating from the shelf can be traced in the DWBC as far downstream as the latitude of Cape Farewell, where the anomalously fresh oxygenated plumes are repeatedly observed in the ISOW and DSOW density classes.

The results of our analysis along with the results from earlier studies [e.g., Rudels et al., 1999; Rudels et al., 2002] indicate that shelf water cascading in the northern Irminger Sea is an intermittent process occurring in all seasons of the year. This implies that, despite the apparent short duration of a particular cascading event, the cumulative contribution of such events to the thermohaline variability and southward export of the deep waters in the WBC can be considerable. Our tentative estimate based on data from two synoptic surveys at $\sim 59.5^\circ\text{N}$ suggests that the transient contribution of a cascading event in the northern Irminger Sea to the DWBC transport at Cape Farewell can be as large as $\sim 25\%$.

References

1. Bacon, S. (1998), Decadal variability in the outflow from the Nordic seas to the deep Atlantic Ocean, *Nature*, *394*, 871–874.
2. Dickson, R. R., and J. Brown (1994), The production of North Atlantic Deep Water: Sources, rates and pathways, *J. Geophys. Res.*, *99*, C6, 12319–12341.
3. Dickson, R., Yashayaev, I., Meincke, J., Turrell, B., Dye, S., and J. Holfort (2002), Rapid freshening of the deep North Atlantic Ocean over the past four decades, *Nature*, *416*, 832–837.
4. Boessenkool, K. P., Hall, I. R., Elderfield, H., and I. Yashayaev (2007), North Atlantic climate and deep-ocean flow speed changes during the last 230 years, *Geophys. Res. Lett.*, *34*, L13614, doi:10.1029/2007GL030285.
5. Curry, R., Dickson, R., and I. Yashayaev (2003), A change in the freshwater balance of the Atlantic Ocean over the past four decades, *Nature*, *426*, 826–829.
6. Falina, A., A. Sarafanov, and A. Sokov (2007), Variability and renewal of Labrador Sea Water in the Irminger Basin in 1991–2004, *J. Geophys. Res.*, *112*, C01006, doi: 10.1029/2005JC003348.
7. Falina A., A. Sarafanov, H. Mercier, P. Lherminier, A. Sokov, and N. Daniault (2012), On the cascading of dense shelf waters in the Irminger Sea, *J. Phys. Oceanogr.*, doi:http://dx.doi.org/10.1175/JPO-D-12-012.1 (in press)
8. Hansen, B., Osterhus S., Quadfasel D., and W. Turrell (2004), Already the day after tomorrow?, *Science*, *305*, 953–954.
9. Hurrell, J. W. (1995), Decadal trends in the North Atlantic Oscillation: regional temperatures and precipitation, *Science*, *269*, 676–679.
10. Koltermann, K. P., A. Sokov, V. Tereschenkov, S. Dobroliubov, K. Lorbacher, and A. Sy (1999), Decadal changes in the thermohaline circulation of the North Atlantic, *Deep Sea Res., Part II*, *46*, 109–138, doi:10.1016/S0967-0645(98)00115-5.
11. Lherminier, P., H. Mercier, T. Huck, C. Gourcuff, F. F. Perez, P. Morin, A. Sarafanov, and A. Falina (2010), The Atlantic Meridional Overturning Circulation and the subpolar gyre observed at the A25–Ovide section in June 2002 and 2004, *Deep-Sea Res., Part I*, *57*, 1374–1391, doi:10.1016/j.dsr.2010.07.009.

12. Meehl, G. A., (2007), Global climate projections. *Climate Change 2007: The Physical Science Basis*, S. Solomon et al., Eds., Cambridge University Press, 747–847.
13. Pickart, R. S., Spall, M., Ribergaard, M. H., Moore, G. W. K. and R. Milliff (2003), Deep convection in the Irminger Sea forced by the Greenland tip jet, *Nature*, *424*, 152–156.
14. Rudels B., Eriksson P., Grönvall H., Hietala R. and Launiainen J. (1999), Hydrographic Observations in Denmark Strait in Fall 1997, and their Implications for the Entrainment into the Overflow Plume, *Geophys. Res. Lett.*, *26*, 1325–1328.
15. Rudels, B., E. Fahrbach, J. Meincke, G. Budeus, and P. Eriksson (2002), The East Greenland Current and its contribution to the Denmark Strait overflow, *ICES J. Marine Science*, *59*, 1133–1154.
16. Sarafanov, A., A. Sokov, A. Demidov, and A. Falina (2007), Warming and salinification of intermediate and deep waters in the Irminger Sea and Iceland Basin in 1997–2006, *Geophys. Res. Lett.*, *34*, L23609, doi:10.1029/2007GL031074.
17. Sarafanov, A., A. Falina, A. Sokov, and A. Demidov (2008), Intense warming and salinification of intermediate waters of southern origin in the eastern subpolar North Atlantic in the 1990s to mid-2000s, *J. Geophys. Res.*, *113*, C12022, doi:10.1029/2008JC004975.
18. Sarafanov, A. (2009), On the effect of the North Atlantic Oscillation on temperature and salinity of the subpolar North Atlantic intermediate and deep waters, *ICES J. Marine Science*, *66* (7), 1448–1454, doi:10.1093/icesjms/fsp094.
19. Sarafanov, A., A. Falina, H. Mercier, P. Lherminier, and A. Sokov (2009), Recent changes in the Greenland–Scotland overflow-derived water transport inferred from hydrographic observations in the southern Irminger Sea, *Geophys. Res. Lett.*, *36*, L13606, doi:10.1029/2009GL038385.
20. Sarafanov A., A. Falina, P. Lherminier, H. Mercier, A. Sokov, and C. Gourcuff (2010a), Assessing decadal changes in the Deep Western Boundary Current absolute transport southeast of Cape Farewell (Greenland) from hydrography and altimetry, *J. Geophys. Res.*, *115*, C11003, doi:10.1029/2009JC005811.
21. Sarafanov A., H. Mercier, A. Falina, A. Sokov, and P. Lherminier (2010b), Cessation and partial reversal of deep water freshening in the northern North Atlantic: observation-

- based estimates and attribution, *Tellus*, 62A, 80–90, doi:10.1111/j.1600-0870.2009.00418.x.
22. Sarafanov A., A. Falina, H. Mercier, A. Sokov, P. Lherminier, C. Gourcuff, S. Gladyshev, F. Gaillard, and N. Danialt (2012) Mean full-depth summer circulation and transports at the northern periphery of the Atlantic Ocean in the 2000s, *J. Geophys. Res.*, 117, C01014, doi:10.1029/2011JC007572.
 23. Schmitz, W. J., Jr., and M. S. McCartney (1993), On the North Atlantic Circulation, *Rev. Geophys.*, 31, 29–49.
 24. Schott, F. A., and P. Brandt (2007), Circulation and deep water export of the subpolar North Atlantic during the 1990s, in *Ocean Circulation: Mechanisms and Impacts*, *Geophys. Monograph Series*, 173, Eds. A. Schmittner, J. Chiang, and S. Hemmings, 91–118, doi:10.1029/173GM08.
 25. Sutherland, D. A., and R. S. Pickart (2008), The East Greenland Coastal Current: structure, variability, and forcing, *Prog. Oceanogr.*, 78, 58–77, doi:10.1016/j.pocean.2007.09.006.
 26. Våge K., R. Pickart, A. Sarafanov, Ø. Knutsen, H. Mercier, P. Lherminier, H. van Aken, J. Meincke, D. Quadfasel, and S. Bacon (2011a), The Irminger Gyre: circulation, convection, and interannual variability, *Deep-Sea Res. Part I*, 58, 590–614, doi:10.1016/j.dsr.2011.03.001.
 27. van Aken, H. M. (2007), *The oceanic thermohaline circulation: An introduction*, New York, Springer, 326 p., ISBN 978-0-387-36637-1.
 28. Yashayaev, I. (2007), Hydrographic changes in the Labrador Sea, 1960–2005, *Prog. Oceanogr.*, 73, 242–276.

1.5 Preliminary Results

The upper-ocean, mid-depth and deep water circulation patterns, merging the results of the present analysis with those from the earlier studies [e.g., *Macrander et al.*, 2005; *Østerhus et al.*, 2005, 2008; *Schott and Brandt*, 2007; *Sutherland and Pickart*, 2008; *Lherminier et al.*, 2010; *Våge et al.*, 2011], are schematically visualized Figures 12–14. A schematic diagram of the meridional overturning circulation in the Atlantic Ocean north of 59.5°N is displayed in Fig. 9.

The results provide the following conceptual view of the gyre / overturning circulation at the northern periphery of the Atlantic Ocean in the 2000s.

The NAC and IC collectively carry 21.1 ± 1.0 Sv of warm upper-ocean waters across 59.5°N northwards within the MOC σ upper limb ($\sigma_0 < 27.55$). About 40% of this flow forms the Atlantic Inflow to the Nordic Seas, and 60% (12.7 ± 1.4 Sv) recirculates westwards in the subpolar gyre northern limb south of Iceland to feed the WBC in the Irminger Sea. Only 20% (2.4 ± 1.2 Sv) of the recirculating NAC/IC-derived waters exits the Irminger Sea in the WBC at shallow levels ($\sigma_0 < 27.55$), while 80% (10.2 ± 1.7 Sv, a half of the NAC/IC northward flow across 59.5°N) gains density of $\sigma_0 > 27.55$ and enters the MOC σ lower limb. The resulting net southward transport in the MOC σ lower limb at the latitude of Cape Farewell is 16.5 ± 2.2 Sv, of which ~60% (~10.2 Sv) is due to light-to-dense water transformation south of the GSR.

As no dense-to-light water re-conversion is expected to occur in the subpolar gyre, the NAC/IC-derived waters, once entering the MOC σ lower limb in the Irminger Sea, will eventually contribute to the MOCz lower limb (~11 Sv at 59.5°N) at the southern margin of the subpolar region. There, at ~48°N, the MOC σ and MOCz are of nearly the same magnitude, 16 ± 2 Sv, as estimated from data collected in the 1990s [see *Schott and Brandt*, 2007; *Lumpkin et al.*, 2008]. This is very close to our estimate of the mean MOC σ at 59.5°N. The comparison is tentative, though, because it does take into account the decadal variability of the MOC [Koltermann *et al.*, 1999; Willis, 2010]. With this caveat in mind, our results imply a minor contribution to the MOC σ by the net dense water formation in the subpolar gyre between ~48°N and 59.5°N. This inference concurs with the results by *Pickart and Spall* [2007] suggesting a

minor contribution to the Atlantic MOC by the net water mass transformation in the Labrador Sea.

To conclude, the results of the present study, verified with independent estimates where possible, provide the first observation-based quantitative view of a mean state of the gyre / overturning circulation at the northern periphery of the Atlantic Ocean. The most interesting features of the obtain circulation pattern are as follows:

- Nearly half of volume of the upper-ocean waters transported northward across 59.5°N in the eastern limb of the subpolar gyre (NAC and IC, $\sigma_0 < 27.55$) overturns in the density plane south of the GSR and feeds the lower limb of the Atlantic MOC σ .
- The contribution to the MOC σ lower limb at 59.5°N by overturning (light-to-dense transformation) of the NAC / IC-derived upper-ocean waters south of the GSR is one and a half times as large as the contribution of the Nordic Seas overflows.
- The net southward flow in MOC σ lower limb at 59.5°N is associated primarily with the deep water ($\sigma_0 > 27.80$) export. Nearly half of the net southward flow of deep waters across 59.5°N is due to entrainment of the Atlantic waters in the Irminger Sea.
- The DWBC at 59.5°N is fed primarily by the Denmark Strait Overflow and by the diapycnal flux / entrainment from the mid-depth layer, while the contribution to the DWBC transport from the ISOW flow is minor. A major part of the ISOW transported into the Irminger Sea from the Charlie-Gibbs Fracture Zone recirculates southward in the eastern Irminger Sea and exits the basin via an interior pathway rather than along the western boundary. The results can be used for validation of numerical models. From this perspective, multi-year mean transports have an obvious advantage over individual section-based synoptic estimates, which bear the impress of vigorous variability occurring on a variety of spatial and temporal scales. The methodological outcome is that the combined use of repeat hydrography, the MDT by *Rio and Hernandez* [2004] and satellite altimetry data can provide a useful estimate of the mean full-depth circulation across a transatlantic section without imposing *a priori* constraints.

1.6 Major Problems and Goals Not Achieved

Bottle #4 leaked on the first two stations. Seasave did not work properly on sta. Sta ##3171-3173. Due to emergency case we stopped to carry out the section for 15 hours after Sta. #3204. Bottle #19 leaked on Sta #3206. Bottle #3 did not closed on Sta #3211. Restarted TSG on Sta # 3227.

2. CONTINUOUS MEASUREMENTS (on station and underway)

2.1 Navigation

Navigation data from Trimble SPSx50/SPSx51 GPS was recorded every 1 second and was stored on the PC in binary format.

2.2 Meteorological Measurements

The standard mean meteorological measurements were stored in the separate files on the same PC with navigation data. Recording were running immediately after departure from Gdansk (Poland) on 30th June, and worked reliably until completion of the cruise in Iqaluit (Canada) on 19th July.

2.3 Thermosalinograph

SBE 21 S/N 3254 data were collected along the section line starting on July 3rd.

2.4 Echosounding

The bathymetric equipment aboard during RV Akademik Ioffe Cruise 44 consists of an ELAC 12 kHz hydrographic echosounder. Data were collected for most of the cruise. The Hull mounted transducer is located 5.8 metres below the sea surface and this value was entered to estimate the depth.

Depth was indicated on the echosounder display and stored on the PC together with the navigation.

Two files with extension NAV and MET with maximum size 256032 b were created. File name corresponded to GMT time when the file was opened for records.

2.5 Vessel Mounted Acoustic Doppler Current Profiler (VMADCP) OS 38 kHz

The Ocean Surveyor 38 kHz is designed for vessel-mount current profile measurement in the upper ocean water from depths greater than 40-50 meters. The system consists of a transducer and electronics chassis connected to PC. Data are transmitted in binary format through the I/O cable. GPS data in NMEA format are transmitted separately to another PC COM – port. The VMADCP can operate in two regimes (Narrow Bandwidth and Broad Bandwidth Profiling). Its main specifications are shown below.

To collect OS 38 kHz data we used *VmDas* software (version 1.46). The NMEA messages *VmDas* reads are standard GGA, HDG, HDT, VTG messages.

	Bin size	Maximum range	Accuracy (cm/s) ²
NarrowBand (long-range mode)	16 m	800 - 1000 m	30
	24 m	900 - 1200 m	23
BroadBand (high-precision mode)	16 m	520 - 730 m	12
	24 m	730 – 780 m	9

We used a following configuration to collect the data.

NP00001 – Narrow Bandwidth profiling

NN060 – number of bins 60

NS2400– cell size 24 m

NF1600 – blanking size 16 m

BP00 – no bottom track (BP),

VmDas saves data in a few files with extension ENX, ENS, ENR (raw data with and without navigation), NR – NMEA messages, STA and LTA averaged data. Misalignment angle was introduced in configuration file and was used by VmDas for data correction.

Data processing performed STA files with 40-profile averaging. Taking into account that single ping takes about 3 seconds, one 40-profile ensemble lasts near 120 seconds in Narrow Bandwidth regime.

Data processing consists of data conversion in NetCDF format with extension NC and further cleaning, filtering, tide removing (using barotropic tidal model TPXO 7.2) and averaging. The standard averaging was 3 km. IFREMER software was used to process OS 38 kHz data.

3. ON-STATION MEASUREMENTS

3.1 CTD

3.1.1 Equipment

The deep profiler system used during the cruise included the following components: SBE 32 painted aluminum 24 bottle multisampler frame, SBE 9P-0743 CTD, Up and Down looking RD Instruments WHS – 300 kHz Acoustic Doppler Current Profiler (LADCP), Separate Battery pack pressure case ext. 6000 m connected to LADCPs with star cable, 24 x 5 liter Test Oceanic Niskin bottles, Benthos altimeter PSA-900D.

Lab equipment for data acquisition and archiving of CTD/LADCP data consisted of the following items mounted on the deck.

Pentium IV – Intel 2.2 GHz, PC Intel Core 2 Duo 2.4GHz Personal Computers. APC Back-UPS 550VA/330W, SBE 11p Deck Unit.

Cruise Preparation

Equipment and sensors were assembled when the ship crossed the Baltic and North Seas (1-4th July). Water bottles were checked for integrity of seals, taps, stoppers and lanyards before being fitted and roped to the multisampler frame.

Deployment

The CTD was deployed with a lowering rate of 60 meters/min (30-40 meters/min in the upper 200 meters or deeper if the conditions are rough). It is recovered at a rate of 60 meters/min.

The LADCPs fitted within the frame with a separate battery pressure case performed well. These units contain a compass and tilt sensors which could possibly provide useful information on the attitude and rotation of the whole profiler package throughout deployments.

Bottle firing using the deck unit and pylon was very reliable during the cruise.

Operationally this has been a successful cruise with virtually no time being lost due to mechanical or equipment failure.

3.1.2 Data processing and calibration

CTD data were logged at 24 scans per second and passed from the CTD deck unit to the PC.

The CTD data was recorded onto disk by the PC using SEABIRD SEASOFT-Win 32: Seasave 7, Software Release 7.21d. A screen display of temperature, oxygen, salinity and density profiles vs pressure are used to decide the depths at which bottles are to be tripped on the up cast. The bottles are tripped using the enable and fire buttons on the PC screen. During post-processing, the SEASAVE software stores 35 scans at each bottle trip within a separate file. At the end of the station, all the data and header files associated with the station are transferred immediately via ethernet to the second PC. The SBE data processing software is used to create 1 dbar processed data files.

The data processing takes the following steps:

DATCNV Converts the raw data to physical parameters.

WILDEDIT For every block of 100 scans, flags all scans whose pressure, temperature, conductivity and oxygen values differ from the mean by more than 2 standard deviations. Recomputes mean from unflagged data then marks as bad all scans exceeding 20 standard deviations from these new values.

FILTER Low pass filter pressure channel with time constant used for pressure 0.150 seconds.

ALIGNCTD Aligns the oxygen values relative to the pressure values accounting for the time delays in the system. Time offsets of 4.000 secs for oxygen are used.

CELLTM A recursive filter used to remove the thermal mass effects from the conductivity data. Thermal anomaly amplitude and time constants of 0.0300 and 7.0000 were used.

LOOPEDIT Marks as bad, all cycles on the down trace for which the vertical velocity of the CTD unit is less than 0.25 metres/sec.

WINDOW FILTER cosine filter temperature and conductivity, window size 23 scans.

DERIVE Computes salinity, potential temperature, sigma-t, sigma theta and oxygen values.

BINAVG Averages the down cast into 1 dbar pressure bins.

SPLIT Splits the data into DOWN and UP cast.

Calibration data

The CTD calibrations used during this cruise were supplied by Sea Bird Electronics and are as follows:

Pre-cruise calibration:

CALIBRATION DATE: 24-Jun-2014 (all stations)

Conductivity Sensor 042827

Conductivity = $(g + hf2 + if3 + jf4) / 10(1 + dt + ep)$ Siemens/meter
 t = temperature [$^{\circ}$ C]; p = pressure[decibars]; d = CTcor; e= CPcor;
 g=-1.00348848e+001

$h = 1.36977079e+000$
 $i = 5.01531580e-004$
 $j = 2.74090064e-005$
 $CP_{cor} = -9.5700e-008$
 $CT_{cor} = 3.2500e-006$

Post-cruise calibration:

CALIBRATION DATE: 04-Jun 2015 (all stations)

Conductivity Sensor S/N 042827

$g = -1.00469063e+001$
 $h = 1.37383902e+000$
 $i = -6.26359501e-004$
 $j = 1.11707771e-004$
 $CP_{cor} = -9.5700e-008$
 $CT_{cor} = 3.2500e-006$

Average drift between *pre* and *post-cruise* calibrations: -0.00010 PSU/month

Pre-cruise calibration:

CALIBRATION DATE: 19-Jun-14 (all stations)

Temperature Sensor S/N 035677

Temperature ITS-90 = $1/\{g + h[\ln(f_0/f)] + i[\ln^2(f_0/f)] + j[\ln^3(f_0/f)]\} - 273.15$ (°C)

Following the recommendation of JPOTS: T68 is assumed to be $1.00024 * T90$ (-2 to 35°C)

f is the frequency

$g = 4.29395484e-003$
 $h = 6.23609246e-004$
 $i = 1.89843091e-005$
 $j = 1.41258435e-006$
 $f_0 = 1000.0$

Post-cruise calibration:

CALIBRATION DATE: 19-Jun-14 (all stations)

Temperature Sensor 035677

$g = 4.29395484e-003$
 $h = 6.23609246e-004$
 $i = 1.89843091e-005$
 $j = 1.41258435e-006$
 $f_0 = 1000.0$

Average drift between *pre* and *post-cruise* calibrations: +0.00000 Degrees Celsius/year

Pressure Sensor S/N 89105 (all stations) no drift

CALIBRATION DATE: 27-June-11

$C1 = -4.905371e+004$
 $C2 = -1.210594e+000$
 $C3 = 1.428350e-002$
 $D1 = 3.901600e-002$
 $D2 = 0.000000e+000$
 $T1 = 3.001017e+001$
 $T2 = -5.758384e-004$
 $T3 = 4.210120e-006$
 $T4 = 2.265400e-009$

T5 = 0.0000 0 0 e+000)
 AD590M = 1.28912e-002
 AD590B = -8.43097e+000
 Slope = 0.99995
 Offset = 1.4284 (dbars)

Oxygen Sensor 430699

CALIBRATION DATE: 23-Oct-2014 (All Stations)

$$\text{Oxygen(ml/l)} = \{ \text{Soc} * (V + \text{Voffset}) \} * \text{Oxsat}(T,S) * e^{(\text{Tcorr}*T)} * e^{(\text{Pcor}*P)}$$

Where:

V = SBE 43 output voltage signal (volts)

T = CTD temperature (°C)

S = CTD salinity (psu)

P = CTD pressure (dbars)

Oxsat(T,S) = oxygen saturation (ml/l)

Soc, Voffset, tcor, and pcor are calibration coefficients

Let:

$$\phi = \text{Oxsat}(T,S) * e^{(\text{Tcorr}*T)} * e^{(\text{Pcor}*P)}$$

$$\text{Oxygen(ml/l)} = \text{Soc} * (V + \text{Voffset}) * \phi$$

$$\text{Oxygen(ml/l)} / \phi = \text{Soc} * (V + \text{Voffset}) = M * V + B$$

Where:

$$\text{Soc} = M$$

$$\text{Voffset} = B / M$$

The final coefficients are

$$\text{Soc} = 4.2281\text{e-}001$$

$$\text{Tau} = 0.0$$

$$\text{Boc} = 0.0000$$

$$\text{Voffset} = -0.4317$$

$$\text{tcor} = 0.001700$$

$$\text{pcor} = 1.35\text{e-}004$$

3.1.3 Final Post-Cruise CTD Calibrations

Temperature Calibration Temperature Sensor 035677

Zero sensor drift was applied to the temperature data based on the *pre cruise calibration coefficients* for all stations.

Pressure Calibration Pressure Sensor S/N 89105

Final CTD pressure correction: Since no drift for pressure sensor was defined by SeaBird Electronics pressure was corrected for atmospheric pressure only. With offset in *.con* or *.xmlcon* file set to -0.0026 db, pressure measured by CTD should equal barometric pressure

- Calculate offset (db) = barometer reading – CTD reading
- Conversion of psia to decibars: decibars = (psia - 14.7) * 0.6894759
- Enter calculated offset in *.con* or *.xmlcon* file
- Example:
 - CTD reads -2.5 dbars
 - Barometer reads 14.65 psia.

Converting to decibars, barometer reads (14.65 - 14.7) * 0.6894759 = -0.034 dbars

– offset (db) = barometer reading – CTD reading = -0.034 - (-2.5) = 2.466

Salinity Calibration Conductivity Sensor 042827

We used *pre-cruise calibration coefficients* for all stations of the cruise (sensor slope correction 1.0000000).

3.1.4 SBE 43 Dissolved Oxygen Sensor Calibration using Winkler Titrations

We use a method for statistically estimating calibration coefficients for calculating dissolved oxygen in milliliters per liter from SBE 43 output voltage. The technique requires dissolved oxygen concentration in ml/l (determined from Winkler titration of water samples) and SBE 43 oxygen voltage outputs at the times the water samples were collected. Sea-Bird's data processing software, SBE Data Processing, is used to produce a data table suitable for the analysis.

Background

The equation used in Sea-Bird's software for calculating dissolved oxygen in ml/l from SBE 43 output voltage is a form of that given in Owens-Millard (1985):

$$Oxygen(ml/l) = \{Soc * (V + Voffset + tau * \partial V/\partial t) + Boc * e^{(-0.03*T)}\} * Oxsat(T,S) * e^{(Tcorr*T)} * e^{(Pcor*P)}$$

eqn 1

Where:

V = SBE 43 output voltage signal (volts)

$\partial V/\partial t$ = time derivative of SBE 43 output signal (volts/second)

T = CTD temperature ($^{\circ}\text{C}$)

S = CTD salinity (psu)

P = CTD pressure (dbars)

$O_{xsat}(T,S)$ = oxygen saturation (ml/l)

Soc , Boc , $Voffset$, tau , $tcor$, and $pcor$ are calibration coefficients

Characterization of the SBE 43 in the laboratory and ocean suggest that the most accurate results are obtained by setting Boc and tau to zero. Equation 1 then reduces to:

$$Oxygen(ml/l) = \{Soc * (V + Voffset)\} * O_{xsat}(T,S) * e^{(Tcor*T)} * e^{(Pcor*P)} \quad eqn 2$$

The SBE 43 is expected to provide an output voltage that is linear with respect to oxygen concentration. Normal calibration drift manifests itself as a loss of sensitivity and is evident as a change of slope and offset in the linear relationship between oxygen concentration and voltage output. The coefficients $tcor$ and $pcor$ correct for small secondary responses to temperature and pressure. Because these coefficients change very slowly over time, the values given on the SBE 43 calibration certificate are used in this analysis.

Setting Boc and tau to zero, we will rearrange equation 2 into a linear form and perform a linear regression to obtain a new Soc and $Voffset$.

Let:

$$\phi = O_{xsat}(T,S) * e^{(Tcor*T)} * e^{(Pcor*P)}$$

The oxygen equation then reduces to:

$$Oxygen(ml/l) = Soc * (V + Voffset) * \phi$$

This may be expressed in a linear form as shown in equation 3 below. A linear regression is calculated using Winkler oxygen concentration divided by ϕ as the dependent variable and SBE 43 output voltage as the independent variable.

$$Oxygen(ml/l) / \phi = Soc * (V + Voffset) = M * V + B \quad eqn 3$$

Where:

$$Soc = M$$

$$Voffset = B / M$$

Winkler oxygen divided by ϕ versus SBE 43 output voltage for this cruise is shown in **Fig. 11** and includes a linear regression line calculated from the data.

The $Soc = 4.19326e-001$

The $Voffset = -0.4297$ for the transatlantic section along 59.5 N

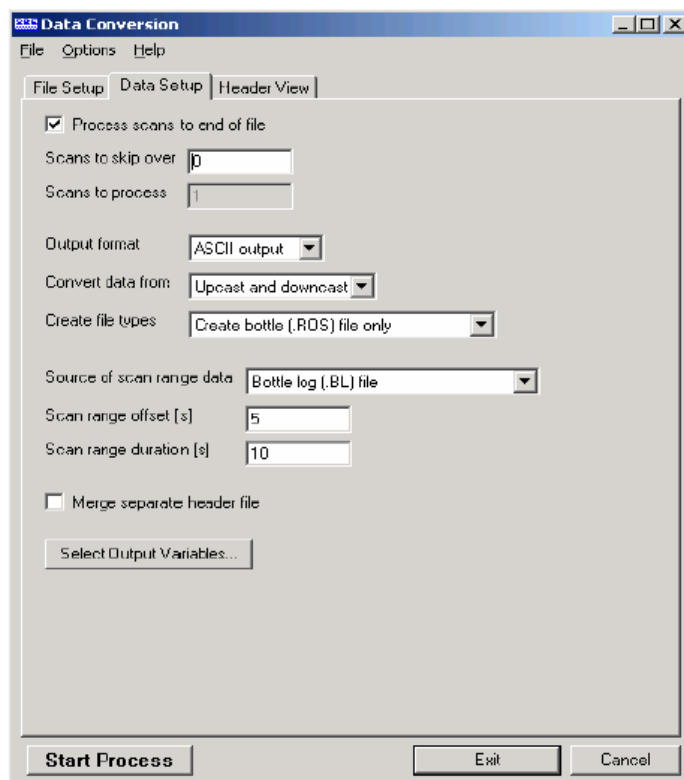
1251 oxygen samples were used to build this linear fit for the 59.5 N line.

Procedure

As a first step, extract pressure, temperature, salinity, oxygen saturation, and SBE 43 voltage from the parts of your CTD data collected when the water sampler closures occurred.

We run SBE Data Processing, and select Data Conversion in the Run menu. Select the appropriate configuration (*.con*) and data (*.dat*) files on the *File Setup* tab. In the *Data Setup* tab we set *Convert data from* to *Upcast and downcast* and *Create file types* to *Create bottle (.ros) file only*.

To extract CTD data concurrent to the water sampler closures, Data Conversion must know when the closures occurred. Select an appropriate *Source of scan range data*, depending on your instrument type and how the sampler was commanded to close bottles:



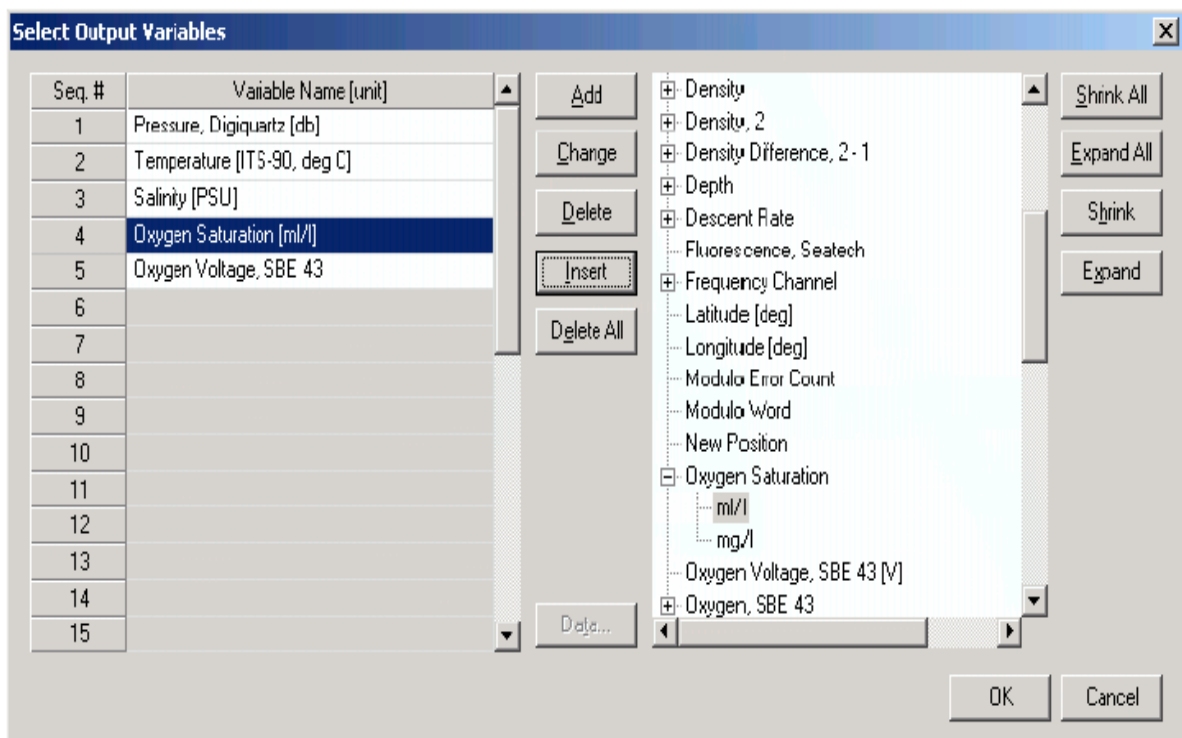
- SBE 9plus with SBE 11plus - The data stream is marked with a *bottle confirm* bit each time a closure occurred.

- Using SEASAVE to operate the water sampler - A *.bl* file, with scan ranges corresponding to closures, is created during the cast.

Like all sensors, the SBE 43 has a finite response time to a change in dissolved oxygen concentration. This response time is usually on the order of 6 seconds. For this reason, good sampling procedure dictates that the instrument package should be stopped in the water column long enough for the SBE 43 and all other sensors to completely equilibrate before closing the water sampler. An equilibration time of 5 to 6 response times, or 30 to 36 seconds, is adequate. We used to wait 30 seconds.

Data Conversion is extracting data 5 seconds before each water sampler closure and will extract 10 seconds of data. Note that 10 seconds is longer than the SBE 43 response time. Because we are extracting data for 5 seconds after the water sampler closure, the instrument package must remain stopped for at least this long.

To estimate *Soc* and *Voffset*, we need pressure, temperature, salinity, oxygen saturation (ml/l), and SBE 43 Oxygen Voltage to go with each Winkler titration data value. We use *Select Output Variables* and add each of the required parameters; the dialog box is shown below.



After selecting all the variables, click *OK* to return to the Data Conversion Data Setup tab. Then click *Start Process* to create the *.ros* file.

In our case, the *.ros* file contains 10 seconds of data centered on the moment the bottle closure occurred for every bottle closure. To make a useful table, we select Rosette Summary from SBE Data Processing's Run menu. Rosette Summary calculates averages and standard deviations for the variables selected in Data Conversion. Select the appropriate *.con* and *.ros* files on the *File Setup* tab. To average the data in the *Data Setup* tab we click the *Select Averaged Variables* button; after selecting all the variables, click *OK* to return to the Rosette Summary Data Setup tab. Then click *Start Process* to create a data table file with the *.bt1* extension.

Further, we run a program READBT1DATA to create a file with average pressure, temperature, salinity, oxygen saturation, and SBE 43 output voltage for each water sampler closure depth, by importing the *.bt1* file and the Winkler titration dissolved oxygen values from our titration log, matching water sampler closures to number of station, bottle number and pressures. The program also calculates ϕ , using *tcor* and *pcor* from the SBE 43 calibration sheet.

Then, calculate *Winkler O₂/ ϕ* .

Using the table we perform a linear regression, with:

- *Winkler O₂/ ϕ* (shown as Winkler/phi in the table) as the *Y* data
- SBE 43 output voltages as the *X* data

Reference

Owens, W. B., and R. C. Millard Jr., 1985: A new algorithm for CTD oxygen calibration. *J. Phys. Oceanogr.*, 15, 621-631.

(NOTE: calibration expressed as ml/l)

3.2 Oxygen Bottle Samples

Oxygen samples were drawn first from every bottle. Duplicate samples were taken on each cast, usually from the first two bottles. Samples were drawn into clear, wide necked calibrated glass bottles and fixed on deck with reagents dispensed using Aquastep bottle top dispensers. A test station used to check on the oxygen bottle calibrations and as an opportunity to train a number of people to take the samples. The samples were shaken on deck and again in the laboratory 1/2 hour after collection, when the bottles were checked for the tightness of the stoppers and presence of bubbles. The samples were then stored under water until analysis.

Bottle temperatures were taken, following sampling for oxygen, using a hand held electronic thermometer probe. The temperatures were used to calculate any temperature-dependent changes in the sample bottle volumes.

Samples were analyzed in the constant temperature laboratory, starting three hours after sample collection, following the Winkler whole bottle titration with an amperometric method of endpoint detection, as described by Culberson (1991). The equipment used was supplied by Metrohm and included the Titrino unit and control pad, exchange unit with 10 ml burette to dispense the thiosulphate in increments of 2 μ l, with an electrode for amperometric end point detection.

The difference for the duplicate pairs sampled on each station was in a range 0.00-0.02 ml/l (Table 2).

The thiosulphate normality was checked on each run and recalculated every time the reservoir was topped up against potassium iodate. The exact weight of this standard, the calibrated 5 ml exchange unit driven by a Metrohm Dosimat and the 1L glass volumetric flask used to dispense and prepare the standard.

The introduction of oxygen with the reagents and impurities in the manganese chloride were corrected for by blank measurements made on each run, as described in the WOCE Manual of Operations and Methods (Culberson, 1991).

Collected data shows that dissolved oxygen concentrations varied from 4.81 to 9.10 ml/l. In order to control the accuracy of the oxygen measurements at each cast were taken parallel samples from the 1-2 bottles or duplicate samples.

Reproducibility of measurements

1395 samples were taken during the cruise; in addition 53 duplicates were analyzed. These include both duplicates taken from the same bottle (replicates) and those taken from different bottles fired at the same depth. The data gave a standard deviation of 0.005 ml/l.

3.3 Nutrient Bottle Samples

Samples for nutrient measurements were collected following oxygen samples from each Niskin bottle. Water was collected in clean plastic containers that had been rinsed three times by seawater through the latex tube.

Concentrations of silicate and phosphate were determined by photometric methods with spectrophotometer Cary 100 Seam Varian. All samples were analyzed immediately after sampling.

Silicate determined by Korolev's method based on colorimeter of blue silicomolybdic complex (methodology described in Modern methods..., 1992). The ascorbic acid used as a restorative. The absorbance was read at 810 nm. Relative error of this method on concentration of dissolved silicate at 4.5 μ M is $\pm 4\%$, on concentration at 45 μ M - $\pm 2,5\%$. Measured concentrations were in a range from 0.20 to 20.71 μ M.

Phosphates determined according to the method Murphy and Raily (Modern methods..., 1992). Phosphate, dissolved in sea water, react with ammonium molybdate in a presence of sulfuric acid and tartrate potassium-antimony. The generated complex aggregate of phosphomolybdic heteropolyacid and trivalent antimony restorative by the ascorbic acid, and then determined the absorbance at 885 nm (we use the cavity 10cm). Relative error of this method $\pm 1\%$.

In order to ensure accuracy and increase precision of determination 3-8 duplicate samples were analyzed at each run. The mean difference for the duplicate pairs sampled on each station was in an error limits of the methods (Table 2).

References:

Culberson, C.H. 1991.15 pp in the WOCE Operations Manual (WHP Operations and Methods) WHPO 91/1, Woods Hole.

Modern methods of hydrochemical research of the ocean, 1992. IO RAS, Moscow (in Russian).

(L. Dukhova)

3.4 Lowered Acoustic Doppler Current Profiler (LADCP)

The TRDI WHS 300 kHz ADCPs consists of a pressure case rated to 6000 meters with 4 transducers at one end in a convex arrangement and the beams diverging at 20 degrees from the vertical. At the opposite end to the transducers is a connector that enables downloading of data and connects it to other pressure cases containing another ADCP and the power supply pack. This arrangement allowed the ADCPs and the battery pack to be mounted vertically as up and down-looking on the CTD frame. Connection amongst all units was established using star cable with three male and two female terminations. Two male cable ends were always attached to the frame, this enabled comms leads to be readily connected pre and post deployment.

Communications: The 20-m communication leads (which also allow external power to be supplied to the ADCP) were sufficiently long to route it through to the port side of the deck lab where it was connected to a dedicated PC and external power supply. The latter was set at 48+ volts and was left on whilst the ADCP was on deck. 5 minutes prior to deployment the external power supply was shut off, the instrument checked and the configuration file sent to the ADCP as described in the manual instructions. The free end of the fly leads was greased and the end cap refitted, this was then taped to the frame for security.

Post deployment: When the CTD/LADCP was brought inboard, the fly-lead connectors were dried and the comms leads were connected to them. This stopped undue bending of the cables and kept them clear of the water bottles, aiding sampling. External power was applied again and the cast data downloaded as per the manual with a baud rate of 57600. The processing is accomplished using software developed by Visbeck after transferring the data to the PC.

Battery power was supplied to the ADCP in the form of 42 volts from 28 x 1.5 volt alkaline cells. Four of these packs were available for the cruise, as the ADCP will function at a minimum of 32 volts this was deemed an adequate stock for the duration.

Data quality: The data quality from the ADCP was good throughout. Due to the bad weather instrument titles sometimes exceeded 12° and this data was rejected during processing.

The LADCPs seem to function well and generates useful information on currents. The battery supply has its limitations though and thought should be given to alternatives to the present set-up.

3.4.1 LADCP Processing for Current Profiles

A brief account of the LADCP current data processing, file nomenclature and directory structure is provided in the following lines. Little emphasis is put into a detailed description of the main programming tools used, since these are part of a standard software package developed by Gerd Krahnemann (version 10.13).

Outline of LADCP current calculation method

The Broad Band LADCP used during AI41 cruise was designed to measure the instantaneous relative velocities of scatterers in the water column by taking advantage of the Doppler frequency shift, phase changes and correlation between coded pulses transmitted and received by the LADCP's four transducers. Conversion of this raw data stream to a profile of absolute currents involved an elaborate calculation method.

Firstly, Doppler shifts needed to be scaled to velocity units by taking into account the depth-dependent sound velocity (estimated from CTD T and S measurements). Directions could be inferred from trigonometric calculations based on the geometry of the transducer set, the orientation of the package (measured with a flux gate compass) and the local magnetic declination. The depth of the instrument was calculated from the integration of the measured vertical velocity and later adjusted to match the depth given by the CTD's pressure sensor.

The velocities corresponding to each single ensemble (or, in effect, to each transducer ping) were gridded in bins of depth set 10 meters. Statistical rejection of spiky measurements within each of these bins followed.

In order to reject the unwanted motion of the instrument (but also the barotropic component of the current), shear profiles were calculated for each ensemble. A complicated editing scheme preceded this shear calculation. A final shear profile (baroclinic current) was derived by real- depth gridding of the shear profiles calculated for individual ensembles. It was hoped that any relative velocities introduced by the high-frequency motion of the CTD package would be smoothed out by this repeated averaging.

The barotropic component of the flow was finally calculated from bottom-tracking measurements (bottom-track mode) or, in most occasions, in an integral sense from differential GPS positions of the ship (water-track mode).

The definitive velocity profile was hence obtained as the sum of the baroclinic and barotropic components.

During AI44 cruise, no specific error calculation was performed. Profiles of shear standard deviation were included in the cast log sheet folder. Internal wave signals were obvious throughout the cruise.

Relevant PC files

The raw data were downloaded from the LADCP into a devoted PC after each cast and stored as a binary file called vNNNNm_01.000 for Master and vNNNNs_01.000 for Slave the c:\ladcp\AI44\dNNN directory, where NNNN stands for the CTD cast number, e.g. raw data from cast 2967 were stored in the files d:\AI44\data\ladcp\v2967m_01.000 and v2967s_01..000.

The configuration files (named Mconf.txt and Sconf.txt) containing the operating instructions (setting of track mode, bin depth, etc.) given to the LADCP previously to deployment was stored in the same directory.

Text files of the form NNNNm.log and NNNNs.log are the log of the 'bbtalk' session (testing the state and functioning of the instrument) previous to deployment. The details of the sessions for every single cast in the cruise are to be found in the cast log sheets.

A whole variety of files were created and manipulated during the different processing stages, and no mention will be made of the majority of them for reasons of clarity. The processing procedure may be summarised in two steps:

- 1- create CTD pressure, temperature and salinity data file as well as navigation collected every second in order to obtain the best possible estimates of depth and sound velocity. This is done using 'SBE Data Processing software and ConvLADCP Fortran program.

2- use the Gerd Krahnmann's standard matlab package (v.10.13) with P. Lherminier's improvements (LPO, IFREMER) to process LADCP and CTD data

References

M. Visbeck 2002 Deep Velocity Profiling using Lowered Acoustic Doppler Current Profiler: Bottom Track and Inverse Solutions *J. Atmos. Oceanic Technol.* 10, 764-773.

3.5 Carbonate System Measurements

The QUIMA-ULPGC group has been invited by Drs. Sokov and Gladyshev from Shirshov Institute of Oceanology (SIO), Russian Academy of Science to collaborate in the project "Interannual monitoring of thermohaline and current structure along 59.5° N for evaluation of climate change in the North Atlantic" inside the hydrographic section CLIVAR A5930N (A1E), as responsible of the carbon parameters measurements. This is the sixth time that the group has been invited to participate in the project. Four member of the group participate in the cruise, Dr. J. Magdalena Santana-Casiano, Dr. Melchor González-Dávila and two students of the Faculty of Marine Science at the ULPGC. The data treatment and discussions of the results are responsibility of Dr. J. M. Santana-Casiano and Dr. Melchor González-Dávila

From 30-6-2014 to 19-7-2014 the Oceanography Cruise AI44 took place on board R/V Akademik Ioffe departing from the Gdansk harbor. The section 59.5°N, (CLIVAR A1E) from Europe to Greenland. Two sections was done.

3.5.1 Measured parameters

In both sections three parameters of the carbon dioxide system were measured along the water column in order to achieve the highest level of data quality and resolution: the pH, the total alkalinity and the total dissolved inorganic carbon.

- The pH was measured in total scale, $\text{pH}_{\text{T},15^{\circ}\text{C}}$, by the UV-Vis spectrophotometric technique using the m-cresol purple as a dye (Clayton and Byrne, 1993).

- The total alkalinity, AT in $\mu\text{mol kg}^{-1}$ was measured by potentiometry (Mintrop et al., 2000).

- The total dissolved inorganic carbon, CT in $\mu\text{mol kg}^{-1}$, was measured using a VINDTA 3C system by coulombimetry (Mintrop et al., 2000).

3.5.2 Sampling procedure

500 ml glass bottles were used for the determination of AT and CT. 100 ml glass bottles were used to analyse pH. The bottles were rinsed twice with seawater and over-filled with seawater. Samples were preserved from the light and analysed between stations. In shallow stations and in case the samples are not possible to be analysed for CT in less than 5 hours after sampling, they were poisoned with HgCl₂ (60 µl, saturated solution).

CRM (batch 117) were used for the AT and CT quality control.

3.5.3 Stations and parameters sampled

A total of 76 stations have been done considering the section, with 1355 Niskin bottles closed and 1385 Niskin sampled (the non-repetitive one) for the carbon dioxide parameters. 1355 samples were analyzed by UV-Vis spectrophotometric pH, 53 for Total alkalinity (manual) and 1320 for Total alkalinity (VINDTA) and 1320 for Total dissolved inorganic carbon.

References

- Mintrop, L., Pérez, F.F., González-Dávila, M., Santana-Casiano, J.M., Körtzinger, A., 2000. Alkalinity determination by potentiometry: Intercalibration using three different methods, *Ciencias Marinas* 26, 23-37.
- Clayton, T. D. Byrne, R.H., 1993. Spectrophotometric seawater pH measurements: total hydrogen ion concentration scale calibration of m-cresol purple and at-sea results, *Deep Sea Res. I* 40, 2115-2129.

(Dr. J. M. Santana-Casiano)

3.6 Phytoplankton production in the North Atlantic

Subpolar North Atlantic is the region of high biological productivity, seasonal and interannual variability. North Atlantic ecosystem is very sensitive to the climate changes. Thus, improving of our representations about spatial and temporal variability of phytoplankton production characteristics is the necessary for understanding of carbon circle patterns and for primary production algorithms evaluations.

The main aims of the studies were:

1. Estimation of primary production and chlorophyll spatial variability and finding relations between phytoplankton production characteristics and circulation as well as patterns of hydrophysical and hydrochemical vertical structure.
2. Measurements of integral phytoplankton production characteristics between Shetlands, Faroes and Iceland as well as in vicinity of 60° N.
3. Study of vertical primary production and chlorophyll distribution.
4. Spatiotemporal primary production, chlorophyll and environmental factors database development.
5. Development of regional primary production models.
6. Improving the estimation of phytoplankton physiological condition by fluorescence methods.
7. Estimation of the dissolved organic matter contribution in primary production.
8. Research of light stress influence on phytoplankton photosynthetic activity.

Phytoplankton production parameters were collected on 76 CTD stations. Vertical distribution of chlorophyll was studied on 28 stations. Primary production was measured on 12 stations. 280 chlorophyll and 144 primary production samples were treated. Totally 328 measurements of pigment concentration were made respectively.

(Dr. A. Demidov)

. CRUISE LOGISTICS

Mobilization

Mobilization for the cruise took place on the way from Gdansk (Poland) to the first station of the cruise. It took three days. The scientific team arrived at the ship on June 28th.

ACKNOWLEDGEMENTS

The principal scientists would like to thank the Master, officers, crew and scientists of the RV Akademik Ioffe for making this such an enjoyable, as well as successful cruise.

TABLES

Table 1. CTD casts

Table 2. Performance of chemical analysis along 59.5 N sections in the cruise 44AI

FIGURES

Fig. 1 Station location and ship track (in red). The shelf area with depth less than 200 m is shaded

Fig. 2 Vertical distribution of samples along the 59.5 section.

Fig. 3. Schematic diagram of the large-scale circulation in the northern North Atlantic compiled from [Schmitz and McCartney, 1993; Schott and Brandt, 2007; Sutherland and Pickart, 2008; Lherminier et al., 2010]. Abbreviations for the main topographic features, currents and water masses are explained in the legend. The nominal locations of the 59.5°N hydrographic section (1997 – present) and sections across the straits between Greenland, Iceland, Faeroe and Shetland Islands (2011 – present) are shown with the solid green lines.

Fig. 4. Oxygen concentrations (ml/l) in the water column (lower panel) as observed in March–October 1997 in four hydrographic sections (upper panel) ending nearby the southern tip of Greenland. A separate oxygen maximum in the LSW layer (1000–2000 m) in the Irminger Sea at 59.5°N strongly implies local convective renewal of LSW before 1997. Adapted from [Falina et al., 2007].

Fig. 5. Warming and salinification in the northern North Atlantic between the mid-1990s and mid-2000s, as observed at 59.5°N. The figure shows the 2006–1997 temperature (°C, left) and salinity (right) differences on isobaric surfaces in the Irminger Sea and Iceland Basin. Adapted from [Sarafanov et al., 2007].

Fig. 6. Coherence of the decadal salinity changes (1950s – 2000s) of the intermediate (LSW) and deep (ISOW) waters in the northern North Atlantic and their link to the North Atlantic Oscillation (NAO) index. **(a)** Schematic representation of the LSW and ISOW pathways and locations of the Icelandic Low (L) and Azores High (H) centers constituting the NAO dipole pattern. The red dotted line indicates the 59.5°N transatlantic section. **(b)** Salinity time series for LSW in the Labrador Sea [Yashayaev, 2007] and ISOW in the Iceland basin [Boessenkool et al., 2007; Sarafanov et al., 2007] overlaid by the third order polynomial fits. **(c)** Time series of the winter NAO index, after [Hurrell, 1995], overlaid by 7-year running mean and third order polynomial fit. **(d)** Mechanism of the NAO effect on the decadal changes in temperature (T) and salinity (S) of the northern North Atlantic intermediate and deep waters. Positive / negative links shown with the dark / light grey arrows mean that changes in ‘causative’ and ‘consequential’ characteristics have the same / opposite sign(s). The overall effect of the NAO on T and S of the in the water column is negative: persistent NAO decline leads to warming and salinification of the water masses and vice versa, as shown in (b) and (c). Adapted from [Sarafanov, 2009].

Fig. 7. Schematic representation of the upper-ocean circulation and convection intensity in the northern North Atlantic under high (left) and low (right) NAO conditions. Blue (magenta) solid arrows indicate the upper-ocean flows with higher fraction of colder fresher subpolar (warmer saltier subtropical) waters. The main pathways of the Nordic overflow-derived deep waters are shown with the dotted curves. “C” and “E” symbols are used to denote, respectively, the deep convection sites and the domain, where the Atlantic waters are entrained into ISOW. Larger (smaller) circles indicate stronger (weaker) convection. SPG and STG – the subpolar and subtropical gyres, respectively. Adapted from [Sarafanov, 2009].

Fig. 8. The Deep Western Boundary Current (DWBC) transport variability and its link to the convection intensity in the Labrador Sea. **(a)** Locations of the hydrographic sections (1991–2007) and schematic of the deep water circulation in the Irminger Sea. **(b)** The DWBC transport anomalies at Cape Farewell in 1991–2007, $1 \text{ Sv} = 10^6 \text{ m}^3 \text{ s}^{-1}$. The 1994–1997 and 2000–2007 mean anomalies and the 1994–2007 linear trend are shown. **(c)** Anomalies of the DWBC transport at Cape Farewell and the Labrador Sea Water (LSW) thickness in the Labrador Sea in the 1950s–2000s. **(d)** Correlation coefficient (R^2) for the two times series shown in **(c)** at the 0–5-year lag, the LSW thickness leads. The correlation maximum is achieved at the 1–3-year lag. The DWBC transport anomalies in the southern Irminger Sea are foregone by the convection intensity anomalies in the Labrador Sea. Adapted from [Sarafanov et al., 2009].

Fig. 9. Schematic diagram of the Meridional Overturning Circulation (MOC) at the northern periphery of the Atlantic Ocean, northeast of Cape Farewell. The dotted lines refer to the σ_0 isopycnals 27.55 and 27.80. The arrows denote the integral meridional and diapycnal volume fluxes. Where the signs are specified, the positive (negative) transports are northward (southward). The NAC and EGIC transports in the upper layer ($\sigma_0 < 27.55$) at 59.5°N are the throughputs accounting for the recirculations. EGIC – the East Greenland / Irminger Current – refers to the upper part of the Western Boundary Current. Other abbreviations are explained in the legend to **Fig. 3**. Adapted from [Sarafanov et al., 2012].

Fig. 10. Salinity observed in the northwestern Irminger Sea at 64.3°N in February 1998. The σ_0 isopycnals 27.55, 27.70, 27.80 and 27.88 are plotted as the thick black lines; the station locations are marked with the ticks on the top axis. The plot shows fresh dense waters descending (cascading) down the continental slope of Greenland down to the LSW layer ($27.70 < \sigma_0 < 27.80$) and the layer of the Nordic Seas overflow-derived deep waters ($\sigma_0 > 27.80$). Adapted from [Falina et al., 2012].

Fig. 11 Regression line for Winkler oxygen divided by ϕ versus SBE 43 output voltage 59.5 section. Some oxygen data collected at the East Greenland shelf is not well fitted (blue dots).

Fig. 12 The vertical distribution of (a) potential temperature ($^{\circ}\text{C}$) and (b) salinity (c) dissolved oxygen ($\mu\text{mol/kg}$) along 59.5 N in July 2013. Density is shown in black.

R/V AK. IOFFE CRUISE 44

45

Table 1

CLIVAR			UTC		POSITION							
STA	CAST	TYPE	DATE	TIME	CODE	LATITUDE	LONGITUDE	NAV	DEP	BTM	BTL	COMMENTS
3155	1	ROS	070414	1631	BE	59 30.0 N	004 34.4 W	GPS	90	4	8	CTD,LADCP,O2,SiO3,PO4
3155	1	ROS	070414	1649	BO	59 30.0 N	004 35.9 W	GPS	90	4	8	CTD,LADCP,O2,SiO3,PO4
3155	1	ROS	070414	1701	EN	59 29.9 N	004 36.0 W	GPS	90	4	8	CTD,LADCP,O2,SiO3,PO4
3156	1	ROS	070414	1918	BE	59 30.0 N	005 16.8 W	GPS	108	4	8	CTD,LADCP,O2,SiO3,PO4
3156	1	ROS	070414	1935	BO	59 29.9 N	005 17.9 W	GPS	108	4	8	CTD,LADCP,O2,SiO3,PO4
3156	1	ROS	070414	1947	EN	59 29.9 N	005 17.9 W	GPS	108	4	8	CTD,LADCP,O2,SiO3,PO4
3157	1	ROS	070414	2219	BE	59 30.0 N	005 58.6 W	GPS	139	3	8	CTD,LADCP,O2,SiO3,PO4
3157	1	ROS	070414	2235	BO	59 30.0 N	005 59.9 W	GPS	139	3	8	CTD,LADCP,O2,SiO3,PO4
3157	1	ROS	070414	2247	EN	59 30.0 N	005 59.5 W	GPS	139	3	8	CTD,LADCP,O2,SiO3,PO4
3158	1	ROS	070514	0131	BE	59 30.0 N	006 39.8 W	GPS	561	4	16	CTD,LADCP,O2,SiO3,PO4
3158	1	ROS	070514	0149	BO	59 30.0 N	006 39.7 W	GPS	561	4	16	CTD,LADCP,O2,SiO3,PO4
3158	1	ROS	070514	0212	EN	59 29.9 N	006 39.5 W	GPS	561	4	16	CTD,LADCP,O2,SiO3,PO4
3159	1	ROS	070514	0445	BE	59 29.9 N	007 18.8 W	GPS	1066	10	21	CTD,LADCP,O2,SiO3,PO4
3159	1	ROS	070514	0513	BO	59 29.9 N	007 19.9 W	GPS	1066	10	21	CTD,LADCP,O2,SiO3,PO4
3159	1	ROS	070514	0546	EN	59 29.9 N	007 19.7 W	GPS	1066	10	21	CTD,LADCP,O2,SiO3,PO4
3160	1	ROS	070514	0513	BE	59 29.9 N	007 59.3 W	GPS	1133	0	21	CTD,LADCP,O2,SiO3,PO4
3160	1	ROS	070514	0844	BO	59 29.7 N	007 59.7 W	GPS	1133	0	21	CTD,LADCP,O2,SiO3,PO4
3160	1	ROS	070514	0925	EN	59 29.6 N	008 00.1 W	GPS	1133	0	21	CTD,LADCP,O2,SiO3,PO4
3161	1	ROS	070514	0846	BE	59 30.0 N	008 39.6 W	GPS	1365	4	21	CTD,LADCP,O2,SiO3,PO4
3161	1	ROS	070514	1220	BO	59 30.0 N	008 39.8 W	GPS	1365	4	21	CTD,LADCP,O2,SiO3,PO4
3161	1	ROS	070514	1300	EN	59 29.9 N	008 39.5 W	GPS	1365	4	21	CTD,LADCP,O2,SiO3,PO4
3162	1	ROS	070514	1530	BE	59 30.0 N	009 19.6 W	GPS	1486	3	21	CTD,LADCP,O2,SiO3,PO4
3162	1	ROS	070514	1601	BO	59 30.1 N	009 19.5 W	GPS	1486	3	21	CTD,LADCP,O2,SiO3,PO4
3162	1	ROS	070514	1644	EN	59 30.2 N	009 18.5 W	GPS	1486	3	21	CTD,LADCP,O2,SiO3,PO4
3163	1	ROS	070514	1907	BE	59 30.0 N	009 58.6 W	GPS	1027	5	21	CTD,LADCP,O2,SiO3,PO4
3163	1	ROS	070514	1934	BO	59 29.9 N	009 59.9 W	GPS	1027	5	21	CTD,LADCP,O2,SiO3,PO4
3163	1	ROS	070514	2006	EN	59 29.7 N	009 59.4 W	GPS	1027	5	21	CTD,LADCP,O2,SiO3,PO4
3164	1	ROS	070514	2232	BE	59 30.0 N	010 38.9 W	GPS	1524	4	21	CTD,LADCP,O2,SiO3,PO4
3164	1	ROS	070514	2309	BO	59 29.7 N	010 39.9 W	GPS	1524	4	21	CTD,LADCP,O2,SiO3,PO4
3164	1	ROS	070514	2351	EN	59 29.5 N	010 39.8 W	GPS	1524	4	21	CTD,LADCP,O2,SiO3,PO4

3165	1	ROS	070614	0210	BE	59 30.0 N	011 19.0 W	GPS	1611	3	21	CTD,LADCP,O2,SiO3,PO4
3165	1	ROS	070614	0248	BO	59 29.9 N	011 19.1 W	GPS	1611	3	21	CTD,LADCP,O2,SiO3,PO4
3165	1	ROS	070614	0330	EN	59 29.8 N	011 18.1 W	GPS	1611	3	21	CTD,LADCP,O2,SiO3,PO4
3166	1	ROS	070614	0608	BE	59 30.0 N	011 59.7 W	GPS	1482	5	14	CTD,LADCP,O2,SiO3,PO4
3166	1	ROS	070614	0640	BO	59 29.9 N	011 59.8 W	GPS	1482	5	14	CTD,LADCP,O2,SiO3,PO4
3166	1	ROS	070614	0730	EN	59 29.5 N	011 59.7 W	GPS	1482	5	14	CTD,LADCP,O2,SiO3,PO4
3167	1	ROS	070614	0958	BE	59 30.0 N	012 39.7 W	GPS	1364	10	21	CTD,LADCP,O2,SiO3,PO4
3167	1	ROS	070614	1020	BO	59 30.1 N	012 39.8 W	GPS	1364	10	21	CTD,LADCP,O2,SiO3,PO4
3167	1	ROS	070614	1102	EN	59 30.3 N	012 39.9 W	GPS	1364	10	21	CTD,LADCP,O2,SiO3,PO4
3168	1	ROS	070614	1328	BE	59 30.0 N	013 19.3 W	GPS	1312	9	20	CTD,LADCP,O2,SiO3,PO4
3168	1	ROS	070614	1357	BO	59 29.9 N	013 19.9 W	GPS	1312	9	20	CTD,LADCP,O2,SiO3,PO4
3168	1	ROS	070614	1433	EN	59 29.8 N	013 19.9 W	GPS	1312	9	20	CTD,LADCP,O2,SiO3,PO4
3169	1	ROS	070614	1703	BE	59 29.9 N	013 59.6 W	GPS	997	5	21	CTD,LADCP,O2,SiO3,PO4
3169	1	ROS	070614	1722	BO	59 30.0 N	013 59.9 W	GPS	997	5	21	CTD,LADCP,O2,SiO3,PO4
3169	1	ROS	070614	1755	EN	59 30.0 N	013 59.9 W	GPS	997	5	21	CTD,LADCP,O2,SiO3,PO4
3170	1	ROS	070614	2015	BE	59 30.0 N	014 39.0 W	GPS	1004	4	21	CTD,LADCP,O2,SiO3,PO4
3170	1	ROS	070614	2041	BO	59 29.9 N	014 40.0 W	GPS	1004	4	21	CTD,LADCP,O2,SiO3,PO4
3170	1	ROS	070614	2110	EN	59 29.8 N	014 40.0 W	GPS	1004	4	21	CTD,LADCP,O2,SiO3,PO4
3171	1	ROS	070614	2334	BE	59 30.0 N	015 19.2 W	GPS	1531	10	20	CTD,LADCP,O2,SiO3,PO4
3171	1	ROS	070714	0006	BO	59 29.7 N	015 20.1 W	GPS	1531	10	20	CTD,LADCP,O2,SiO3,PO4
3171	1	ROS	070714	0046	EN	59 29.6 N	015 20.3 W	GPS	1531	10	20	CTD,LADCP,O2,SiO3,PO4
3172	1	ROS	070714	0308	BE	59 30.0 N	015 59.1 W	GPS	1540	4	14	CTD,LADCP,O2,SiO3,PO4
3172	1	ROS	070714	0344	BO	59 29.8 N	015 59.8 W	GPS	1540	4	14	CTD,LADCP,O2,SiO3,PO4
3172	1	ROS	070714	0427	EN	59 29.7 N	015 59.8 W	GPS	1540	4	14	CTD,LADCP,O2,SiO3,PO4
3173	1	ROS	070714	0659	BE	59 29.9 N	016 39.7 W	GPS	999	999		CTD,LADCP,O2,SiO3,PO4
3173	1	ROS	070714	0723	BO	59 29.9 N	016 39.9 W	GPS	999	999		CTD,LADCP,O2,SiO3,PO4
3173	1	ROS	070714	0725	EN	59 29.8 N	016 39.9 W	GPS	999	999		CTD,LADCP,O2,SiO3,PO4
3173a	1	ROS	070714	0729	BE	59 29.8 N	016 39.9 W	GPS	1078	9	11	CTD,LADCP,O2,SiO3,PO4
3173a	1	ROS	070714	0729	BO	59 29.8 N	016 39.9 W	GPS	1078	9	11	CTD,LADCP,O2,SiO3,PO4
3173a	1	ROS	070714	0750	EN	59 29.7 N	016 39.9 W	GPS	1078	9	11	CTD,LADCP,O2,SiO3,PO4
3173b	1	ROS	070714	0754	BE	59 29.7 N	016 39.9 W	GPS	1175	2	21	CTD,LADCP,O2,SiO3,PO4
3173b	1	ROS	070714	0758	BO	59 29.7 N	016 39.9 W	GPS	1175	2	21	CTD,LADCP,O2,SiO3,PO4
3173b	1	ROS	070714	0808	EN	59 29.7 N	016 39.9 W	GPS	1175	2	21	CTD,LADCP,O2,SiO3,PO4

3174	1	ROS	070714	1051	BE	59 29.9 N	017 20.0 W	GPS	1762	4	21	CTD,LADCP,O2,SiO3,PO4
3174	1	ROS	070714	1123	BO	59 29.8 N	017 20.0 W	GPS	1762	4	21	CTD,LADCP,O2,SiO3,PO4
3174	1	ROS	070714	1207	EN	59 29.7 N	017 20.0 W	GPS	1762	4	21	CTD,LADCP,O2,SiO3,PO4
3175	1	ROS	070714	1431	BE	59 30.0 N	017 59.4 W	GPS	2185	6	21	CTD,LADCP,O2,SiO3,PO4
3175	1	ROS	070714	1513	BO	59 29.8 N	018 00.2 W	GPS	2185	6	21	CTD,LADCP,O2,SiO3,PO4
3175	1	ROS	070714	1607	EN	59 29.4 N	018 00.9 W	GPS	2185	6	21	CTD,LADCP,O2,SiO3,PO4
3176	1	ROS	070714	1824	BE	59 29.9 N	018 39.3 W	GPS	2733	5	21	CTD,LADCP,O2,SiO3,PO4
3176	1	ROS	070714	1915	BO	59 30.0 N	018 40.4 W	GPS	2733	5	21	CTD,LADCP,O2,SiO3,PO4
3176	1	ROS	070714	2011	EN	59 30.2 N	018 41.1 W	GPS	2733	5	21	CTD,LADCP,O2,SiO3,PO4
3177	1	ROS	070714	2242	BE	59 29.9 N	019 18.9 W	GPS	2702	4	21	CTD,LADCP,O2,SiO3,PO4
3177	1	ROS	070714	2333	BO	59 29.9 N	019 20.3 W	GPS	2702	4	21	CTD,LADCP,O2,SiO3,PO4
3177	1	ROS	070814	0029	EN	59 29.8 N	019 20.6 W	GPS	2702	4	21	CTD,LADCP,O2,SiO3,PO4
3178	1	ROS	070814	0314	BE	59 30.0 N	019 59.0 W	GPS	2767	7	21	CTD,LADCP,O2,SiO3,PO4
3178	1	ROS	070814	0409	BO	59 29.5 N	020 00.1 W	GPS	2767	7	21	CTD,LADCP,O2,SiO3,PO4
3178	1	ROS	070814	0503	EN	59 29.1 N	019 59.8 W	GPS	2767	7	21	CTD,LADCP,O2,SiO3,PO4
3179	1	ROS	070814	0747	BE	59 30.0 N	020 39.7 W	GPS	2823	4	21	CTD,LADCP,O2,SiO3,PO4
3179	1	ROS	070814	0837	BO	59 29.8 N	020 39.5 W	GPS	2823	4	21	CTD,LADCP,O2,SiO3,PO4
3179	1	ROS	070814	0944	EN	59 29.5 N	020 38.9 W	GPS	2823	4	21	CTD,LADCP,O2,SiO3,PO4
3180	1	ROS	070814	1219	BE	59 30.0 N	021 19.6 W	GPS	2855	4	21	CTD,LADCP,O2,SiO3,PO4
3180	1	ROS	070814	1312	BO	59 30.0 N	021 19.5 W	GPS	2855	4	21	CTD,LADCP,O2,SiO3,PO4
3180	1	ROS	070814	1414	EN	59 30.0 N	021 18.8 W	GPS	2855	4	21	CTD,LADCP,O2,SiO3,PO4
3181	1	ROS	070814	1635	BE	59 30.0 N	021 59.6 W	GPS	2743	5	21	CTD,LADCP,O2,SiO3,PO4
3181	1	ROS	070814	1726	BO	59 30.1 N	021 59.6 W	GPS	2743	5	21	CTD,LADCP,O2,SiO3,PO4
3181	1	ROS	070814	1824	EN	59 30.1 N	021 58.9 W	GPS	2743	5	21	CTD,LADCP,O2,SiO3,PO4
3182	1	ROS	070814	2049	BE	59 30.0 N	022 38.9 W	GPS	2497	9	21	CTD,LADCP,O2,SiO3,PO4
3182	1	ROS	070814	2143	BO	59 29.9 N	022 39.9 W	GPS	2497	9	21	CTD,LADCP,O2,SiO3,PO4
3182	1	ROS	070814	2231	EN	59 29.9 N	022 39.7 W	GPS	2497	9	21	CTD,LADCP,O2,SiO3,PO4
3183	1	ROS	070914	0103	BE	59 29.9 N	023 19.0 W	GPS	2391	5	21	CTD,LADCP,O2,SiO3,PO4
3183	1	ROS	070914	0153	BO	59 29.7 N	023 19.5 W	GPS	2391	5	21	CTD,LADCP,O2,SiO3,PO4
3183	1	ROS	070914	0241	EN	59 29.3 N	023 19.3 W	GPS	2391	5	21	CTD,LADCP,O2,SiO3,PO4
3184	1	ROS	070914	0516	BE	59 30.0 N	023 59.1 W	GPS	2522	5	21	CTD,LADCP,O2,SiO3,PO4
3184	1	ROS	070914	0605	BO	59 29.8 N	023 59.4 W	GPS	2522	5	21	CTD,LADCP,O2,SiO3,PO4
3184	1	ROS	070914	0704	EN	59 29.8 N	023 58.4 W	GPS	2522	5	21	CTD,LADCP,O2,SiO3,PO4

3185	1	ROS	070914	0949	BE	59 30.0 N	024 39.7 W	GPS	2562	10	21	CTD,LADCP,O2,SiO3,PO4
3185	1	ROS	070914	1036	BO	59 29.8 N	024 39.7 W	GPS	2562	10	21	CTD,LADCP,O2,SiO3,PO4
3185	1	ROS	070914	1134	EN	59 29.7 N	024 39.3 W	GPS	2562	10	21	CTD,LADCP,O2,SiO3,PO4
3186	1	ROS	070914	1407	BE	59 30.0 N	025 19.5 W	GPS	2497	9	21	CTD,LADCP,O2,SiO3,PO4
3186	1	ROS	070914	1456	BO	59 29.5 N	025 19.5 W	GPS	2497	9	21	CTD,LADCP,O2,SiO3,PO4
3186	1	ROS	070914	1551	EN	59 29.1 N	025 19.4 W	GPS	2497	9	21	CTD,LADCP,O2,SiO3,PO4
3187	1	ROS	070914	1820	BE	59 30.0 N	025 59.3 W	GPS	2324	6	21	CTD,LADCP,O2,SiO3,PO4
3187	1	ROS	070914	1904	BO	59 30.0 N	025 59.6 W	GPS	2324	6	21	CTD,LADCP,O2,SiO3,PO4
3187	1	ROS	070914	1953	EN	59 30.0 N	025 59.1 W	GPS	2324	6	21	CTD,LADCP,O2,SiO3,PO4
3188	1	ROS	070914	2221	BE	59 30.0 N	026 39.2 W	GPS	2234	2	21	CTD,LADCP,O2,SiO3,PO4
3188	1	ROS	070914	2310	BO	59 30.2 N	026 39.3 W	GPS	2234	2	21	CTD,LADCP,O2,SiO3,PO4
3188	1	ROS	070914	2357	EN	59 30.1 N	026 38.7 W	GPS	2234	2	21	CTD,LADCP,O2,SiO3,PO4
3189	1	ROS	071014	0230	BE	59 30.0 N	027 19.3 W	GPS	1898	4	21	CTD,LADCP,O2,SiO3,PO4
3189	1	ROS	071014	0316	BO	59 30.2 N	027 19.7 W	GPS	1898	4	21	CTD,LADCP,O2,SiO3,PO4
3189	1	ROS	071014	0359	EN	59 30.5 N	027 19.2 W	GPS	1898	4	21	CTD,LADCP,O2,SiO3,PO4
3190	1	ROS	071014	0629	BE	59 30.0 N	027 59.3 W	GPS	1967	4	21	CTD,LADCP,O2,SiO3,PO4
3190	1	ROS	071014	0708	BO	59 30.1 N	027 59.6 W	GPS	1967	4	21	CTD,LADCP,O2,SiO3,PO4
3190	1	ROS	071014	0757	EN	59 30.3 N	027 58.8 W	GPS	1967	4	21	CTD,LADCP,O2,SiO3,PO4
3191	1	ROS	071014	1034	BE	59 30.0 N	028 39.9 W	GPS	1697	6	21	CTD,LADCP,O2,SiO3,PO4
3191	1	ROS	071014	1112	BO	59 29.9 N	028 39.9 W	GPS	1697	6	21	CTD,LADCP,O2,SiO3,PO4
3191	1	ROS	071014	1155	EN	59 29.9 N	028 39.8 W	GPS	1697	6	21	CTD,LADCP,O2,SiO3,PO4
3192	1	ROS	071014	1427	BE	59 30.0 N	029 19.8 W	GPS	1421	5	21	CTD,LADCP,O2,SiO3,PO4
3192	1	ROS	071014	1458	BO	59 29.8 N	029 20.1 W	GPS	1421	5	21	CTD,LADCP,O2,SiO3,PO4
3192	1	ROS	071014	1537	EN	59 29.7 N	029 20.3 W	GPS	1421	5	21	CTD,LADCP,O2,SiO3,PO4
3193	1	ROS	071014	1807	BE	59 29.9 N	029 59.6 W	GPS	1418	9	21	CTD,LADCP,O2,SiO3,PO4
3193	1	ROS	071014	1840	BO	59 29.8 N	029 59.8 W	GPS	1418	9	21	CTD,LADCP,O2,SiO3,PO4
3193	1	ROS	071014	1915	EN	59 29.6 N	029 59.8 W	GPS	1418	9	21	CTD,LADCP,O2,SiO3,PO4
3194	1	ROS	071014	2213	BE	59 30.0 N	030 39.2 W	GPS	1518	4	21	CTD,LADCP,O2,SiO3,PO4
3194	1	ROS	071014	2247	BO	59 29.8 N	030 39.8 W	GPS	1518	4	21	CTD,LADCP,O2,SiO3,PO4
3194	1	ROS	071014	2322	EN	59 29.7 N	030 39.8 W	GPS	1518	4	21	CTD,LADCP,O2,SiO3,PO4
3195	1	ROS	071114	0152	BE	59 30.0 N	031 19.5 W	GPS	1759	4	21	CTD,LADCP,O2,SiO3,PO4
3195	1	ROS	071114	0228	BO	59 29.8 N	031 20.0 W	GPS	1759	4	21	CTD,LADCP,O2,SiO3,PO4
3195	1	ROS	071114	0307	EN	59 29.6 N	031 20.0 W	GPS	1759	4	21	CTD,LADCP,O2,SiO3,PO4

3196	1	ROS	071114	0522	BE	59 30.0 N	031 59.3 W	GPS	1872	4	21	CTD,LADCP,O2,SiO3,PO4
3196	1	ROS	071114	0605	BO	59 30.2 N	031 59.7 W	GPS	1872	4	21	CTD,LADCP,O2,SiO3,PO4
3196	1	ROS	071114	0647	EN	59 30.4 N	031 59.4 W	GPS	1872	4	21	CTD,LADCP,O2,SiO3,PO4
3197	1	ROS	071114	0910	BE	59 29.9 N	032 39.7 W	GPS	2132	2	21	CTD,LADCP,O2,SiO3,PO4
3197	1	ROS	071114	0952	BO	59 29.9 N	032 40.0 W	GPS	2132	2	21	CTD,LADCP,O2,SiO3,PO4
3197	1	ROS	071114	1044	EN	59 29.8 N	032 40.1 W	GPS	2132	2	21	CTD,LADCP,O2,SiO3,PO4
3198	1	ROS	071114	1258	BE	59 29.9 N	033 19.7 W	GPS	2185	3	21	CTD,LADCP,O2,SiO3,PO4
3198	1	ROS	071114	1341	BO	59 29.8 N	033 20.2 W	GPS	2185	3	21	CTD,LADCP,O2,SiO3,PO4
3198	1	ROS	071114	1434	EN	59 29.6 N	033 20.6 W	GPS	2185	3	21	CTD,LADCP,O2,SiO3,PO4
3199	1	ROS	071114	1653	BE	59 29.9 N	033 59.5 W	GPS	2458	7	21	CTD,LADCP,O2,SiO3,PO4
3199	1	ROS	071114	1744	BO	59 29.5 N	034 00.3 W	GPS	2458	7	21	CTD,LADCP,O2,SiO3,PO4
3199	1	ROS	071114	1840	EN	59 29.3 N	034 00.7 W	GPS	2458	7	21	CTD,LADCP,O2,SiO3,PO4
3200	1	ROS	071114	2056	BE	59 29.9 N	034 39.7 W	GPS	2791	5	21	CTD,LADCP,O2,SiO3,PO4
3200	1	ROS	071114	2146	BO	59 30.0 N	034 39.9 W	GPS	2791	5	21	CTD,LADCP,O2,SiO3,PO4
3200	1	ROS	071114	2239	EN	59 30.2 N	034 39.7 W	GPS	2791	5	21	CTD,LADCP,O2,SiO3,PO4
3201	1	ROS	071214	0100	BE	59 30.0 N	035 19.2 W	GPS	1938	3	21	CTD,LADCP,O2,SiO3,PO4
3201	1	ROS	071214	0140	BO	59 29.8 N	035 20.1 W	GPS	1938	3	21	CTD,LADCP,O2,SiO3,PO4
3201	1	ROS	071214	0222	EN	59 29.6 N	035 20.4 W	GPS	1938	3	21	CTD,LADCP,O2,SiO3,PO4
3202	1	ROS	071214	0438	BE	59 29.9 N	035 59.2 W	GPS	3089	4	21	CTD,LADCP,O2,SiO3,PO4
3202	1	ROS	071214	0537	BO	59 29.9 N	036 00.5 W	GPS	3089	4	21	CTD,LADCP,O2,SiO3,PO4
3202	1	ROS	071214	0640	EN	59 29.9 N	036 01.5 W	GPS	3089	4	21	CTD,LADCP,O2,SiO3,PO4
3203	1	ROS	071214	0856	BE	59 30.0 N	036 39.9 W	GPS	3097	3	21	CTD,LADCP,O2,SiO3,PO4
3203	1	ROS	071214	0953	BO	59 29.9 N	036 40.4 W	GPS	3097	3	21	CTD,LADCP,O2,SiO3,PO4
3203	1	ROS	071214	1059	EN	59 29.9 N	036 40.6 W	GPS	3097	3	21	CTD,LADCP,O2,SiO3,PO4
3204	1	ROS	071214	1317	BE	59 29.9 N	037 19.6 W	GPS	3143	4	21	CTD,LADCP,O2,SiO3,PO4
3204	1	ROS	071214	1417	BO	59 30.0 N	037 20.8 W	GPS	3143	4	21	CTD,LADCP,O2,SiO3,PO4
3204	1	ROS	071214	1526	EN	59 30.2 N	037 21.8 W	GPS	3143	4	21	CTD,LADCP,O2,SiO3,PO4
3205	1	ROS	071314	0805	BE	59 30.0 N	038 00.0 W	GPS	3113	3	21	CTD,LADCP,O2,SiO3,PO4
3205	1	ROS	071314	0905	BO	59 30.2 N	038 00.2 W	GPS	3113	3	21	CTD,LADCP,O2,SiO3,PO4
3205	1	ROS	071314	1014	EN	59 30.6 N	038 00.3 W	GPS	3113	3	21	CTD,LADCP,O2,SiO3,PO4
3206	1	ROS	071314	1237	BE	59 30.0 N	038 39.5 W	GPS	2995	2	21	CTD,LADCP,O2,SiO3,PO4
3206	1	ROS	071314	1340	BO	59 30.1 N	038 40.0 W	GPS	2995	2	21	CTD,LADCP,O2,SiO3,PO4
3206	1	ROS	071314	1448	EN	59 30.2 N	038 39.7 W	GPS	2995	2	21	CTD,LADCP,O2,SiO3,PO4

3207	1	ROS	071314	1718	BE	59 30.0 N	039 19.9 W	GPS	2923	3	21	CTD,LADCP,O2,SiO3,PO4
3207	1	ROS	071314	1812	BO	59 30.1 N	039 19.4 W	GPS	2923	3	21	CTD,LADCP,O2,SiO3,PO4
3207	1	ROS	071314	1915	EN	59 30.2 N	039 19.0 W	GPS	2923	3	21	CTD,LADCP,O2,SiO3,PO4
3208	1	ROS	071314	2142	BE	59 30.0 N	039 59.5 W	GPS	2891	2	21	CTD,LADCP,O2,SiO3,PO4
3208	1	ROS	071314	2239	BO	59 30.0 N	039 59.6 W	GPS	2891	2	21	CTD,LADCP,O2,SiO3,PO4
3208	1	ROS	071314	2335	EN	59 30.0 N	039 59.5 W	GPS	2891	2	21	CTD,LADCP,O2,SiO3,PO4
3209	1	ROS	071414	0159	BE	59 30.0 N	040 39.3 W	GPS	2578	3	21	CTD,LADCP,O2,SiO3,PO4
3209	1	ROS	071414	0251	BO	59 29.9 N	040 39.8 W	GPS	2578	3	21	CTD,LADCP,O2,SiO3,PO4
3209	1	ROS	071414	0344	EN	59 29.9 N	040 39.3 W	GPS	2578	3	21	CTD,LADCP,O2,SiO3,PO4
3210	1	ROS	071414	0502	BE	59 33.8 N	040 59.5 W	GPS	2396	4	21	CTD,LADCP,O2,SiO3,PO4
3210	1	ROS	071414	0547	BO	59 33.9 N	041 00.2 W	GPS	2396	4	21	CTD,LADCP,O2,SiO3,PO4
3210	1	ROS	071414	0636	EN	59 34.0 N	041 00.3 W	GPS	2396	4	21	CTD,LADCP,O2,SiO3,PO4
3211	1	ROS	071414	0744	BE	59 38.5 N	041 15.8 W	GPS	2169	3	21	CTD,LADCP,O2,SiO3,PO4
3211	1	ROS	071414	0829	BO	59 38.6 N	041 16.0 W	GPS	2169	3	21	CTD,LADCP,O2,SiO3,PO4
3211	1	ROS	071414	0922	EN	59 38.5 N	041 16.4 W	GPS	2169	3	21	CTD,LADCP,O2,SiO3,PO4
3212	1	ROS	071414	1033	BE	59 42.5 N	041 31.7 W	GPS	1993	5	21	CTD,LADCP,O2,SiO3,PO4
3212	1	ROS	071414	1115	BO	59 42.5 N	041 31.9 W	GPS	1993	5	21	CTD,LADCP,O2,SiO3,PO4
3212	1	ROS	071414	1203	EN	59 42.5 N	041 31.9 W	GPS	1993	5	21	CTD,LADCP,O2,SiO3,PO4
3213	1	ROS	071414	1310	BE	59 46.5 N	041 46.9 W	GPS	1830	3	20	CTD,LADCP,O2,SiO3,PO4
3213	1	ROS	071414	1351	BO	59 46.6 N	041 47.1 W	GPS	1830	3	20	CTD,LADCP,O2,SiO3,PO4
3213	1	ROS	071414	1438	EN	59 46.5 N	041 46.9 W	GPS	1830	3	20	CTD,LADCP,O2,SiO3,PO4
3214	1	ROS	071414	1553	BE	59 50.8 N	042 03.1 W	GPS	1639	5	19	CTD,LADCP,O2,SiO3,PO4
3214	1	ROS	071414	1629	BO	59 50.2 N	042 03.8 W	GPS	1639	5	19	CTD,LADCP,O2,SiO3,PO4
3214	1	ROS	071414	1712	EN	59 49.5 N	042 03.6 W	GPS	1639	5	19	CTD,LADCP,O2,SiO3,PO4
3215	1	ROS	071414	1750	BE	59 51.5 N	042 06.3 W	GPS	1566	4	20	CTD,LADCP,O2,SiO3,PO4
3215	1	ROS	071414	1822	BO	59 51.0 N	042 06.5 W	GPS	1566	4	20	CTD,LADCP,O2,SiO3,PO4
3215	1	ROS	071414	1905	EN	59 50.7 N	042 07.0 W	GPS	1566	4	20	CTD,LADCP,O2,SiO3,PO4
3216	1	ROS	071414	1947	BE	59 52.1 N	042 09.0 W	GPS	1469	5	18	CTD,LADCP,O2,SiO3,PO4
3216	1	ROS	071414	2018	BO	59 51.8 N	042 09.2 W	GPS	1469	5	18	CTD,LADCP,O2,SiO3,PO4
3216	1	ROS	071414	2053	EN	59 51.5 N	042 09.4 W	GPS	1469	5	18	CTD,LADCP,O2,SiO3,PO4
3217	1	ROS	071414	2134	BE	59 52.6 N	042 11.8 W	GPS	951	2	14	CTD,LADCP,O2,SiO3,PO4
3217	1	ROS	071414	2156	BO	59 52.3 N	042 12.1 W	GPS	951	2	14	CTD,LADCP,O2,SiO3,PO4
3217	1	ROS	071414	2223	EN	59 51.8 N	042 12.8 W	GPS	951	2	14	CTD,LADCP,O2,SiO3,PO4

3218	1	ROS	071414	2252	BE	59 53.4 N	042 15.5 W	GPS	382	5	12	CTD,LADCP,O2,SiO3,PO4
3218	1	ROS	071414	2303	BO	59 53.2 N	042 15.7 W	GPS	382	5	12	CTD,LADCP,O2,SiO3,PO4
3218	1	ROS	071414	2318	EN	59 53.0 N	042 16.1 W	GPS	382	5	12	CTD,LADCP,O2,SiO3,PO4
3219	1	ROS	071414	2347	BE	59 54.0 N	042 19.1 W	GPS	324	4	9	CTD,LADCP,O2,SiO3,PO4
3219	1	ROS	071414	2359	BO	59 53.9 N	042 19.3 W	GPS	324	4	9	CTD,LADCP,O2,SiO3,PO4
3219	1	ROS	071514	0012	EN	59 53.8 N	042 19.5 W	GPS	324	4	9	CTD,LADCP,O2,SiO3,PO4
3220	1	ROS	071514	0034	BE	59 54.2 N	042 22.6 W	GPS	229	4	7	CTD,LADCP,O2,SiO3,PO4
3220	1	ROS	071514	0044	BO	59 54.1 N	042 22.8 W	GPS	229	4	7	CTD,LADCP,O2,SiO3,PO4
3220	1	ROS	071514	0053	EN	59 54.1 N	042 22.8 W	GPS	229	4	7	CTD,LADCP,O2,SiO3,PO4
3221	1	ROS	071514	0112	BE	59 54.4 N	042 26.1 W	GPS	214	5	10	CTD,LADCP,O2,SiO3,PO4
3221	1	ROS	071514	0123	BO	59 54.4 N	042 26.2 W	GPS	214	5	10	CTD,LADCP,O2,SiO3,PO4
3221	1	ROS	071514	0135	EN	59 54.4 N	042 26.1 W	GPS	214	5	10	CTD,LADCP,O2,SiO3,PO4
3222	1	ROS	071514	0200	BE	59 54.6 N	042 29.5 W	GPS	197	5	6	CTD,LADCP,O2,SiO3,PO4
3222	1	ROS	071514	0209	BO	59 54.6 N	042 29.7 W	GPS	197	5	6	CTD,LADCP,O2,SiO3,PO4
3222	1	ROS	071514	0217	EN	59 54.6 N	042 29.6 W	GPS	197	5	6	CTD,LADCP,O2,SiO3,PO4
3223	1	ROS	071514	0241	BE	59 54.8 N	042 33.3 W	GPS	182	5	7	CTD,LADCP,O2,SiO3,PO4
3223	1	ROS	071514	0250	BO	59 54.9 N	042 33.6 W	GPS	182	5	7	CTD,LADCP,O2,SiO3,PO4
3223	1	ROS	071514	0258	EN	59 54.9 N	042 33.4 W	GPS	182	5	7	CTD,LADCP,O2,SiO3,PO4
3224	1	ROS	071514	0319	BE	59 55.2 N	042 36.8 W	GPS	180	5	7	CTD,LADCP,O2,SiO3,PO4
3224	1	ROS	071514	0329	BO	59 55.2 N	042 37.2 W	GPS	180	5	7	CTD,LADCP,O2,SiO3,PO4
3224	1	ROS	071514	0338	EN	59 55.2 N	042 37.1 W	GPS	180	5	7	CTD,LADCP,O2,SiO3,PO4
3225	1	ROS	071514	0357	BE	59 55.6 N	042 40.6 W	GPS	189	5	7	CTD,LADCP,O2,SiO3,PO4
3225	1	ROS	071514	0406	BO	59 55.6 N	042 40.7 W	GPS	189	5	7	CTD,LADCP,O2,SiO3,PO4
3225	1	ROS	071514	0413	EN	59 55.6 N	042 40.7 W	GPS	189	5	7	CTD,LADCP,O2,SiO3,PO4
3226	1	ROS	071514	0442	BE	59 55.8 N	042 44.0 W	GPS	190	4	7	CTD,LADCP,O2,SiO3,PO4
3226	1	ROS	071514	0451	BO	59 55.8 N	042 44.4 W	GPS	190	4	7	CTD,LADCP,O2,SiO3,PO4
3226	1	ROS	071514	0459	EN	59 55.7 N	042 44.5 W	GPS	190	4	7	CTD,LADCP,O2,SiO3,PO4
3227	1	ROS	071514	0523	BE	59 56.1 N	042 47.6 W	GPS	181	5	6	CTD,LADCP,O2,SiO3,PO4
3227	1	ROS	071514	0534	BO	59 56.1 N	042 48.1 W	GPS	181	5	6	CTD,LADCP,O2,SiO3,PO4
3227	1	ROS	071514	0543	EN	59 56.1 N	042 48.4 W	GPS	181	5	6	CTD,LADCP,O2,SiO3,PO4
3228	1	ROS	071514	0604	BE	59 56.6 N	042 51.3 W	GPS	169	1	10	CTD,LADCP,O2,SiO3,PO4
3228	1	ROS	071514	0615	BO	59 56.6 N	042 51.8 W	GPS	169	1	10	CTD,LADCP,O2,SiO3,PO4
3228	1	ROS	071514	0626	EN	59 56.5 N	042 52.2 W	GPS	169	1	10	CTD,LADCP,O2,SiO3,PO4

3229	1	ROS	071514	0648	BE	59 56.9 N	042 55.0 W	GPS	167	4	7	CTD,LADCP,O2,SiO3,PO4
3229	1	ROS	071514	0655	BO	59 56.8 N	042 55.3 W	GPS	167	4	7	CTD,LADCP,O2,SiO3,PO4
3229	1	ROS	071514	0705	EN	59 56.6 N	042 55.5 W	GPS	167	4	7	CTD,LADCP,O2,SiO3,PO4
3230	1	ROS	071514	0730	BE	59 57.3 N	042 59.2 W	GPS	165	5	7	CTD,LADCP,O2,SiO3,PO4
3230	1	ROS	071514	0737	BO	59 57.1 N	042 59.5 W	GPS	165	5	7	CTD,LADCP,O2,SiO3,PO4
3230	1	ROS	071514	0747	EN	59 57.0 N	042 59.7 W	GPS	165	5	7	CTD,LADCP,O2,SiO3,PO4

Table 2

	O ₂ , ml/l	Silicate, μMol kg ⁻¹	Phosphate, μMol kg ⁻¹
Total amount of analyzed samples	1395	1629	1637
Number of duplicates	53	198	206
Mean difference of duplicates	0,005	0,047	0,008
Min difference of duplicates	0,000	0,000	0,000
Max difference of duplicates	0,020	0.236	0,041
Median difference of duplicates	0,003	0,034	0,007
Standard deviation of difference	0,005	0,046	0,007
Accuracy	0,080%	0.780%	0,822%

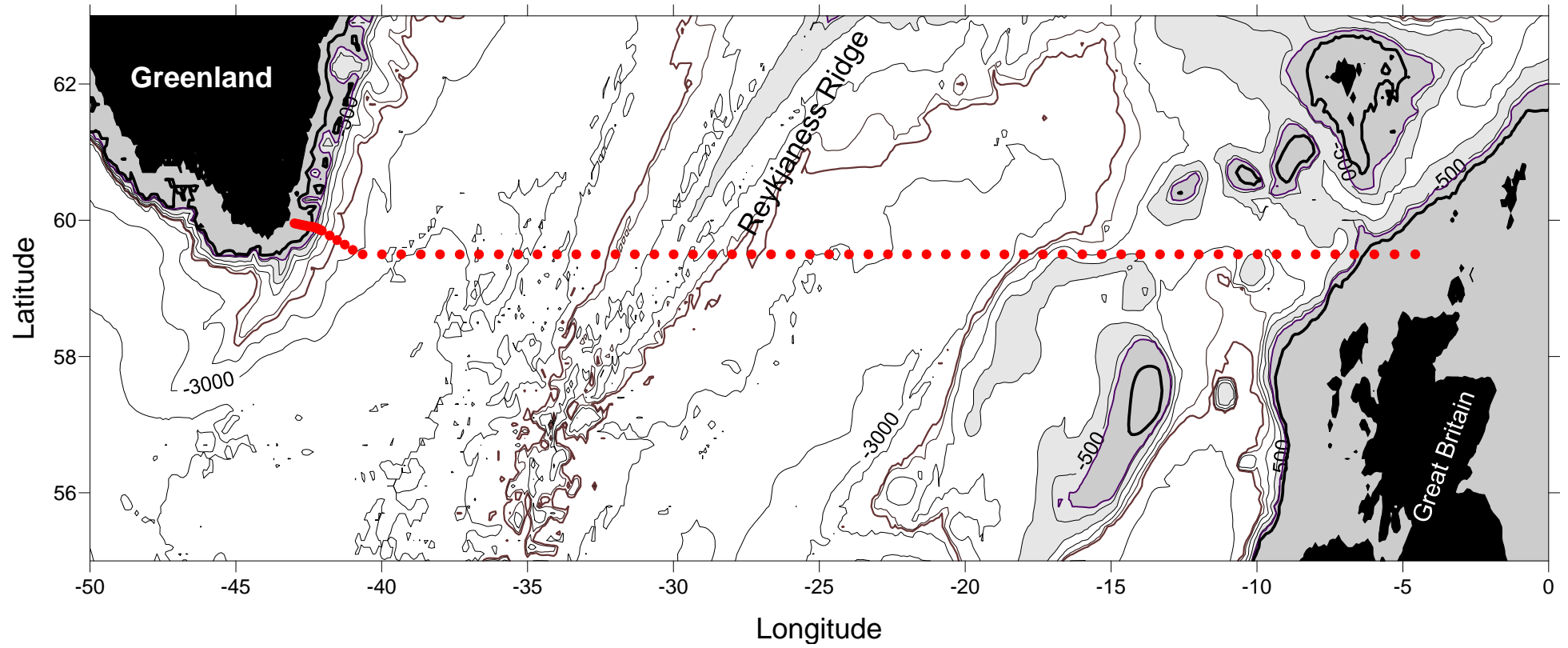


Fig. 1 Station locations (red circles). The shelf area with depth less than 1000 m is shaded.

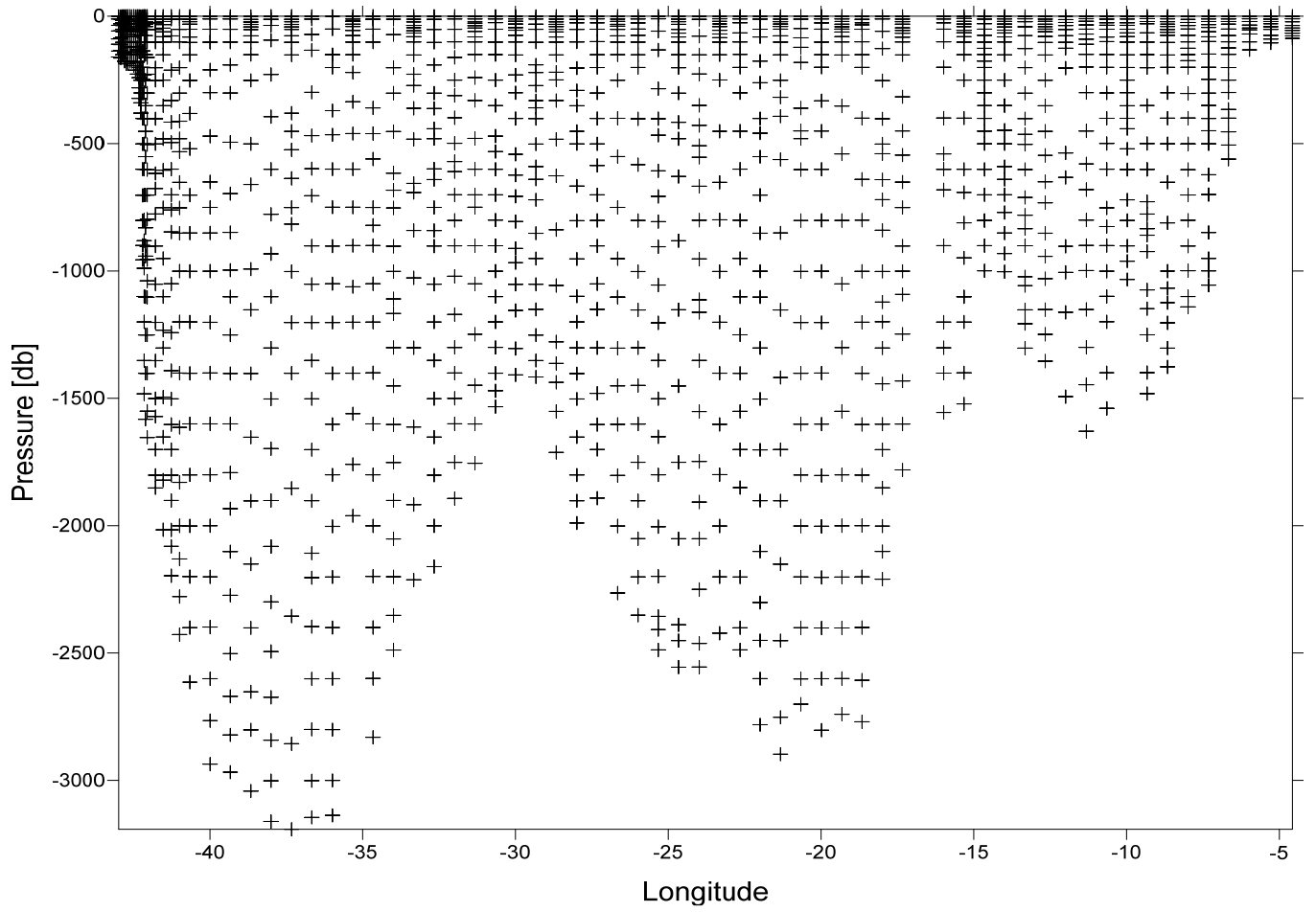


Figure 2. Vertical distribution of samples along the 59.5 section.

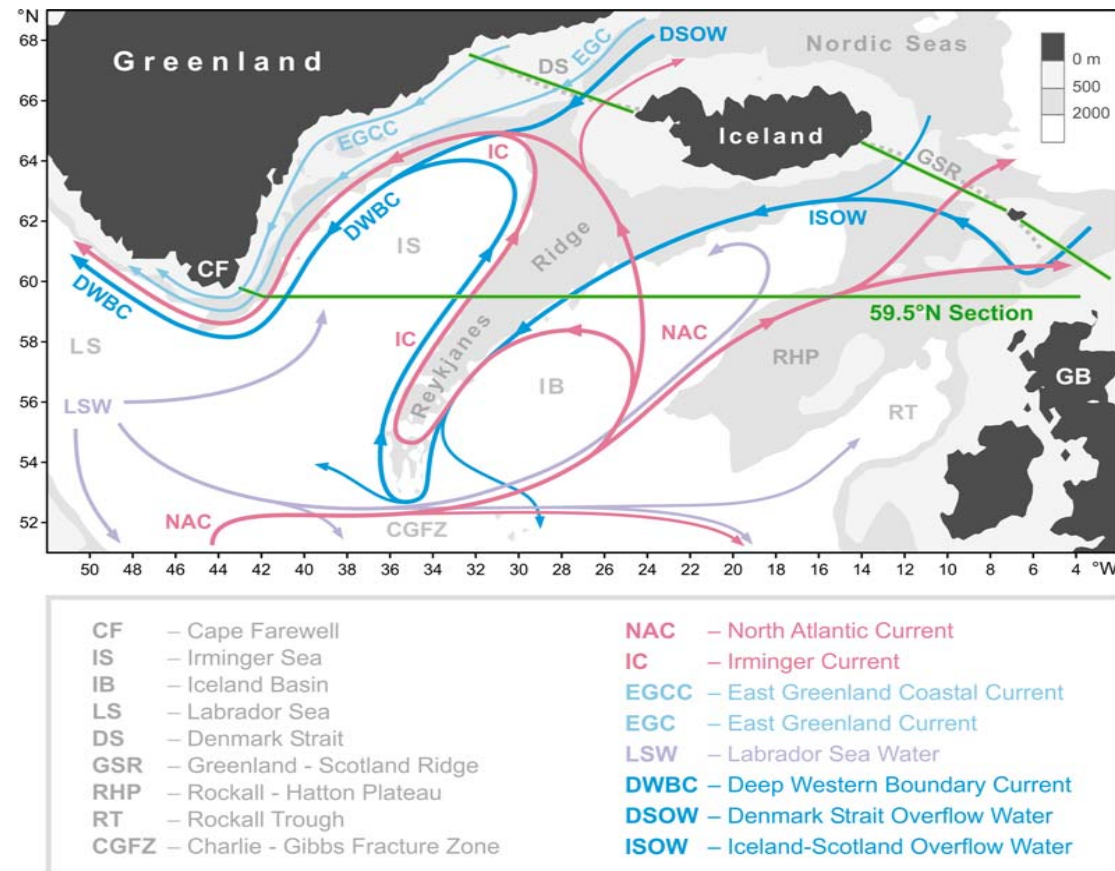


Figure 3. Schematic diagram of the large-scale circulation in the northern North Atlantic compiled from [Schmitz and McCartney, 1993; Schott and Brandt, 2007; Sutherland and Pickart, 2008; Lherminier et al., 2010]. Abbreviations for the main topographic features, currents and water masses are explained in the legend. The nominal locations of the 59.5°N hydrographic section (1997 – present) and sections across the straits between Greenland, Iceland, Faeroe and Shetland Islands (2011 – present) are shown with the solid green lines.

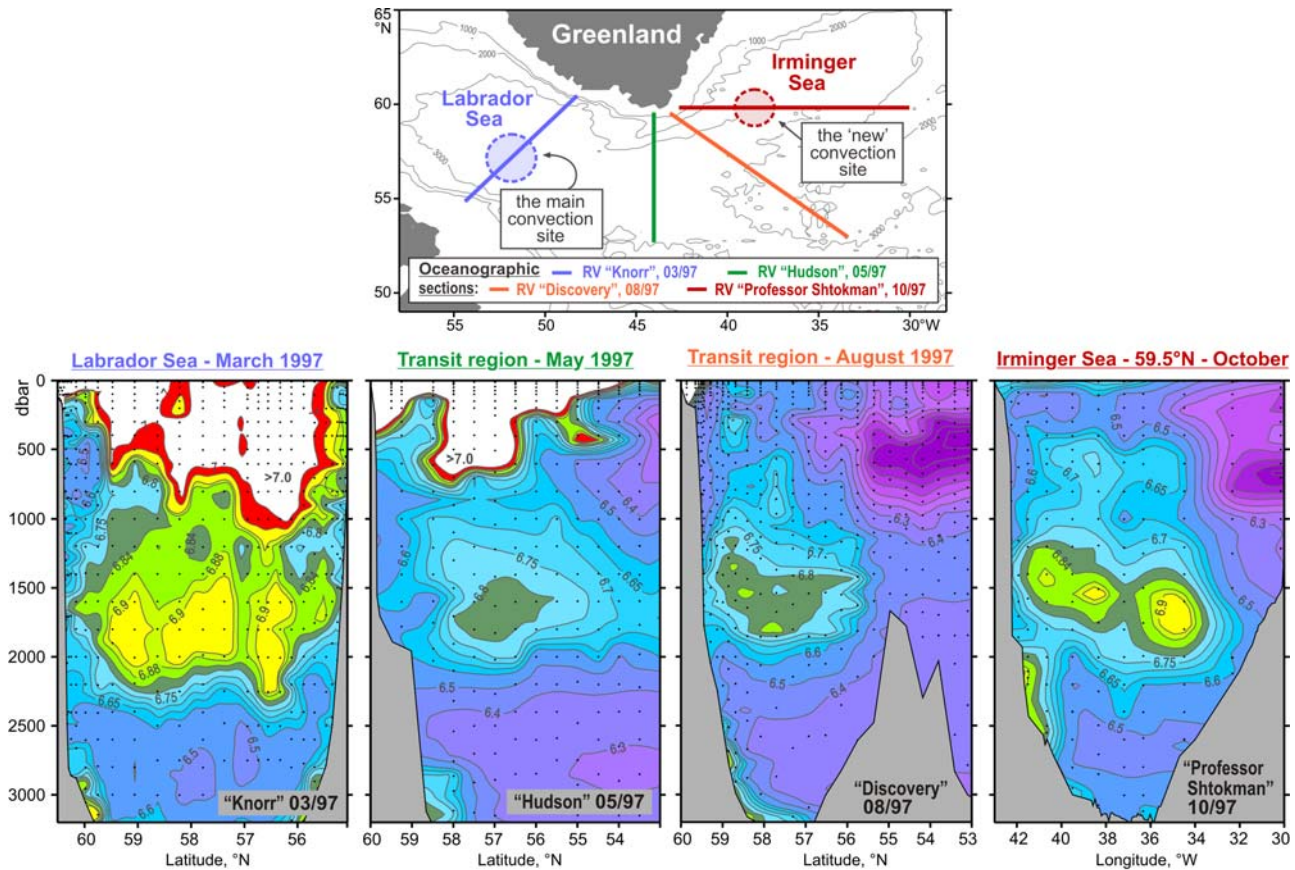


Figure 4. Oxygen concentrations (ml/l) in the water column (lower panel) as observed in March–October 1997 in four hydrographic sections (upper panel) ending nearby the southern tip of Greenland. A separate oxygen maximum in the LSW layer (1000–2000 m) in the Irminger Sea at 59.5°N strongly implies local convective renewal of LSW before 1997. Adapted from [Falina et al., 2007].

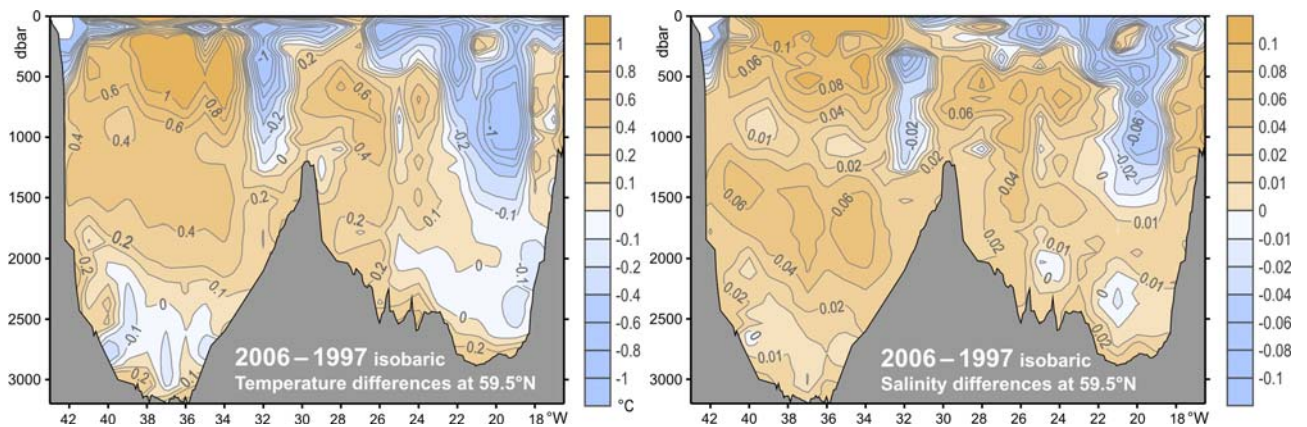


Figure 5. Warming and salinification in the northern North Atlantic between the mid-1990s and mid-2000s, as observed at 59.5°N. The figure shows the 2006–1997 temperature (°C, left) and salinity (right) differences on isobaric surfaces in the Irminger Sea and Iceland Basin. Adapted from [Sarafanov et al., 2007].

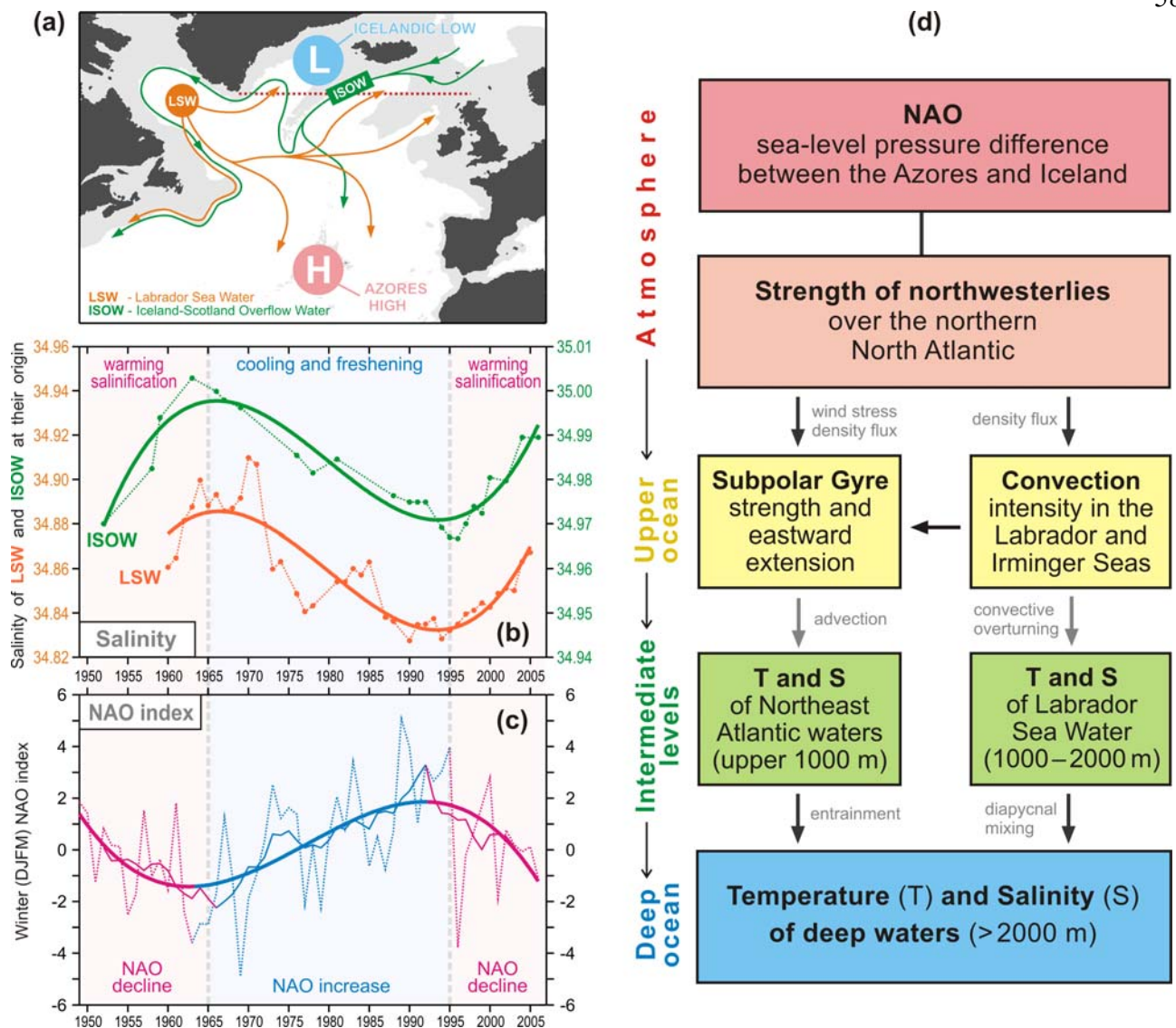


Figure 6. Coherence of the decadal salinity changes (1950s – 2000s) of the intermediate (LSW) and deep (ISOW) waters in the northern North Atlantic and their link to the North Atlantic Oscillation (NAO) index. **(a)** Schematic representation of the LSW and ISOW pathways and locations of the Icelandic Low (L) and Azores High (H) centers constituting the NAO dipole pattern. The red dotted line indicates the 59.5°N transatlantic section. **(b)** Salinity time series for LSW in the Labrador Sea [Yashayaev, 2007] and ISOW in the Iceland basin [Boessenkool et al., 2007; Sarafanov et al., 2007] overlaid by the third order polynomial fits. **(c)** Time series of the winter NAO index, after [Hurrell, 1995], overlaid by 7-year running mean and third order polynomial fit. **(d)** Mechanism of the NAO effect on the decadal changes in temperature (T) and salinity (S) of the northern North Atlantic intermediate and deep waters. Positive / negative links shown with the dark / light grey arrows mean that changes in ‘causative’ and ‘consequential’ characteristics have the same / opposite sign(s). The overall effect of the NAO on T and S in the water column is negative: persistent NAO decline leads to warming and salinification of the water masses and vice versa, as shown in (b) and (c). Adapted from [Sarafanov, 2009].

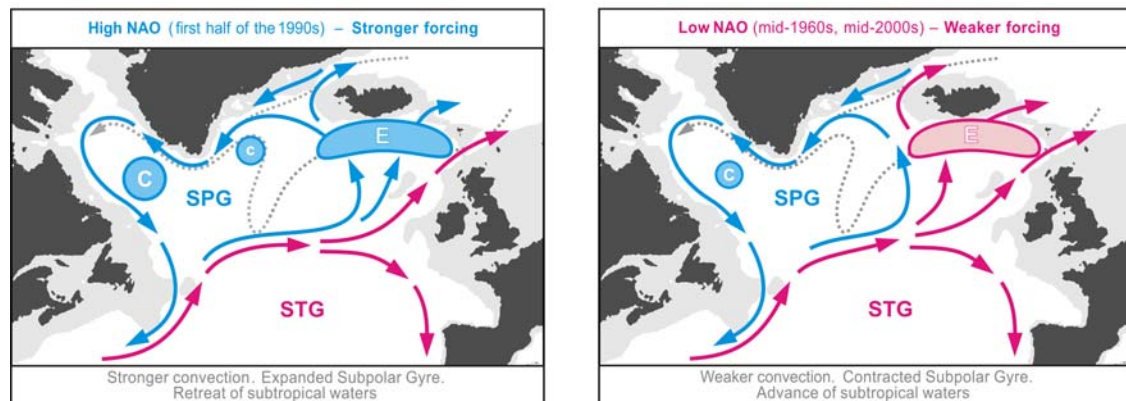


Figure 7. Schematic representation of the upper-ocean circulation and convection intensity in the northern North Atlantic under high (left) and low (right) NAO conditions. Blue (magenta) solid arrows indicate the upper-ocean flows with higher fraction of colder fresher subpolar (warmer saltier subtropical) waters. The main pathways of the Nordic overflow-derived deep waters are shown with the dotted curves. “C” and “E” symbols are used to denote, respectively, the deep convection sites and the domain, where the Atlantic waters are entrained into ISOW. Larger (smaller) circles indicate stronger (weaker) convection. SPG and STG – the subpolar and subtropical gyres, respectively. Adapted from [[Sarafanov, 2009](#)].

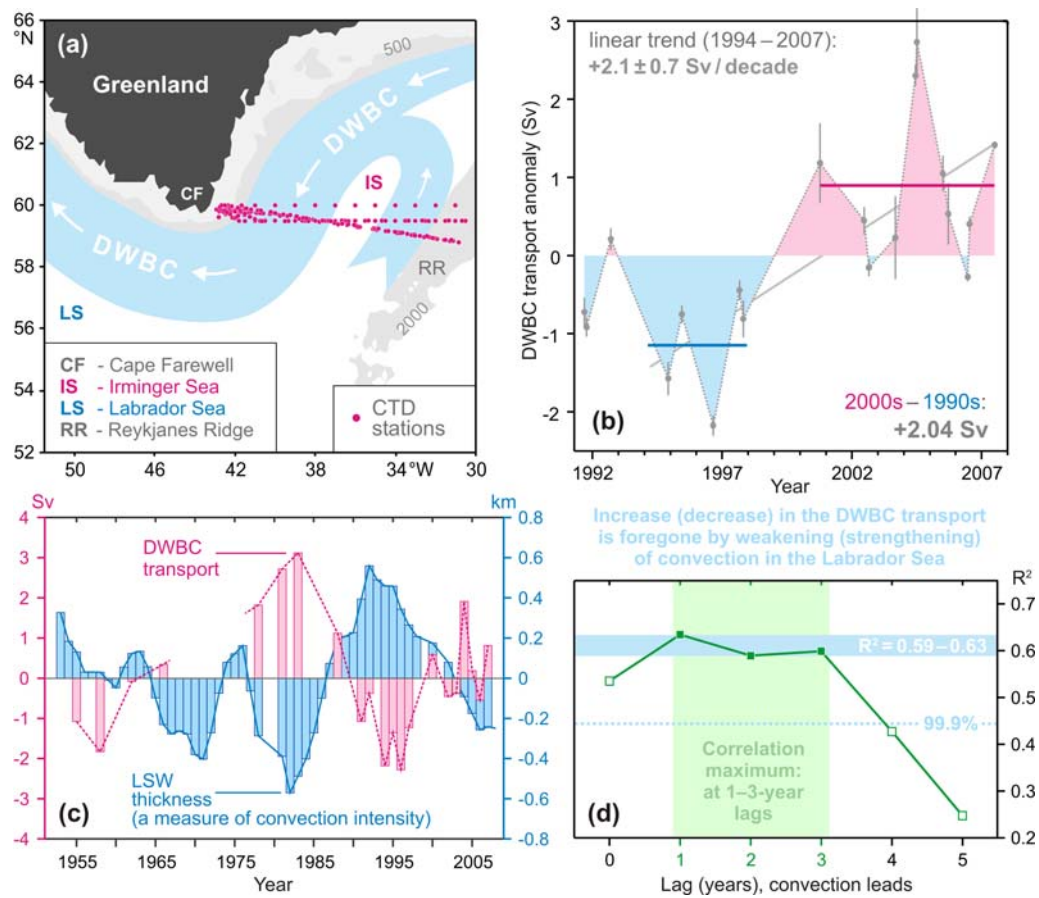


Figure 8. The Deep Western Boundary Current (DWBC) transport variability and its link to the convection intensity in the Labrador Sea. **(a)** Locations of the hydrographic sections (1991–2007) and schematic of the deep water circulation in the Irminger Sea. **(b)** The DWBC transport anomalies at Cape Farewell in 1991–2007, $1 \text{ Sv} = 10^6 \text{ m}^3 \text{ s}^{-1}$. The 1994–1997 and 2000–2007 mean anomalies and the 1994–2007 linear trend are shown. **(c)** Anomalies of the DWBC transport at Cape Farewell and the Labrador Sea Water (LSW) thickness in the Labrador Sea in the 1950s–2000s. **(d)** Correlation coefficient (R^2) for the two time series shown in (c) at the 0–5-year lag, the LSW thickness leads. The correlation maximum is achieved at the 1–3-year lag. The DWBC transport anomalies in the southern Irminger Sea are foregone by the convection intensity anomalies in the Labrador Sea. Adapted from [Sarafanov et al., 2009].

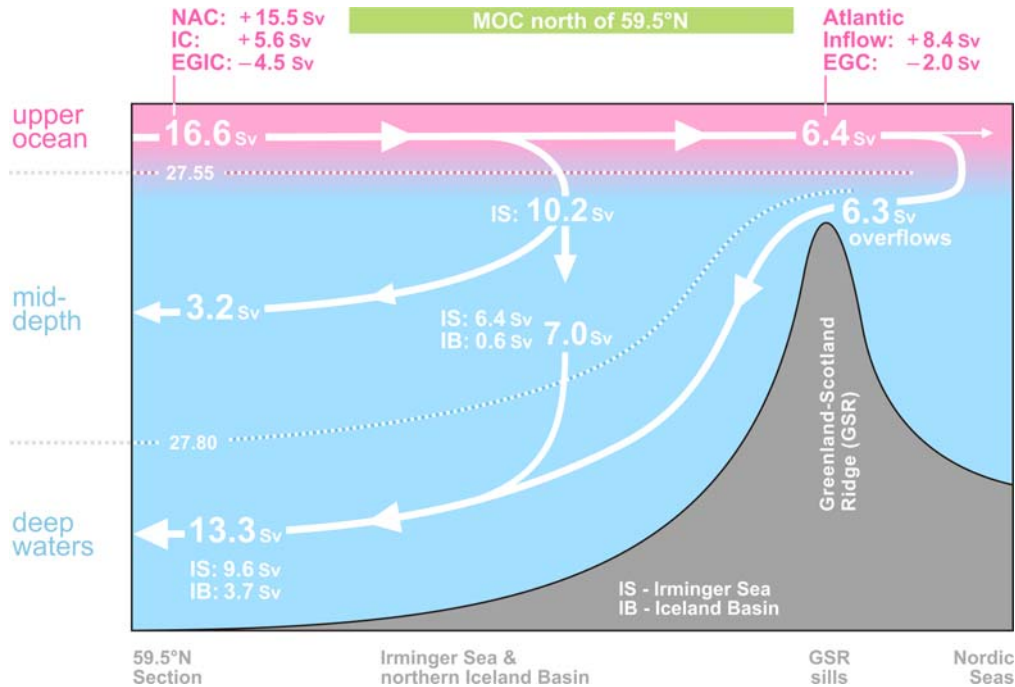


Figure 9. Schematic diagram of the Meridional Overturning Circulation (MOC) at the northern periphery of the Atlantic Ocean, northeast of Cape Farewell. The dotted lines refer to the σ_0 isopycnals 27.55 and 27.80. The arrows denote the integral meridional and diapycnal volume fluxes. Where the signs are specified, the positive (negative) transports are northward (southward). The NAC and EGIC transports in the upper layer ($\sigma_0 < 27.55$) at 59.5°N are the throughputs accounting for the recirculations. EGIC – the East Greenland / Irminger Current – refers to the upper part of the Western Boundary Current. Other abbreviations are explained in the legend to **Figure 3**. Adapted from [Sarafanov et al., 2012].

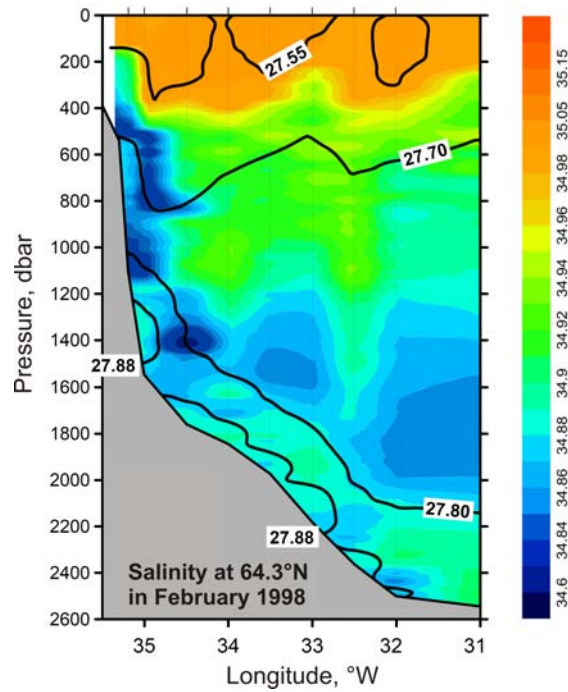


Figure 10. Salinity observed in the northwestern Irminger Sea at 64.3°N in February 1998. The σ_0 isopycnals 27.55, 27.70, 27.80 and 27.88 are plotted as the thick black lines; the station locations are marked with the ticks on the top axis. The plot shows fresh dense waters descending (cascading) down the continental slope of Greenland down to the LSW layer ($27.70 < \sigma_0 < 27.80$) and the layer of the Nordic Seas overflow-derived deep waters ($\sigma_0 > 27.80$). Adapted from [Falina et al., 2012].

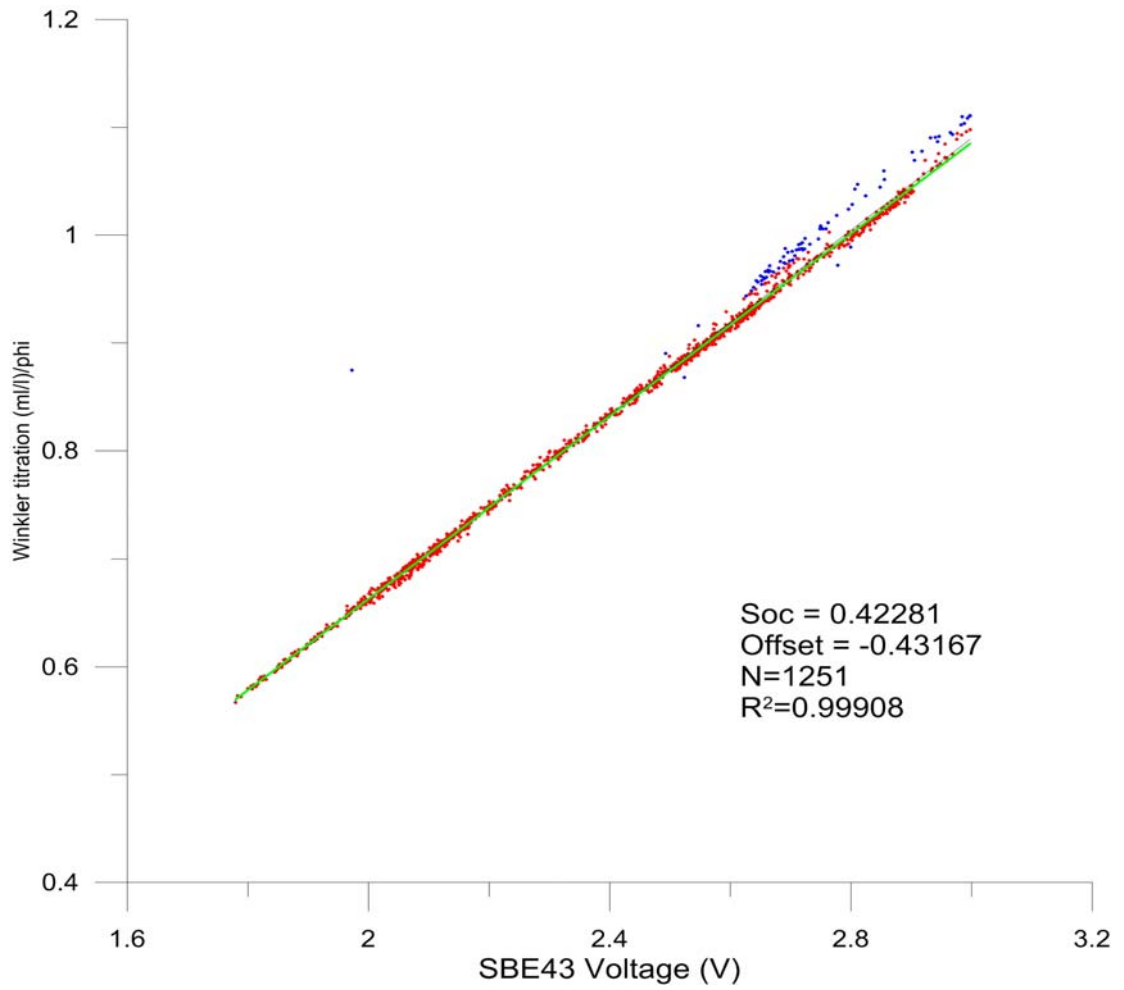


Figure 11 Regression line for Winkler oxygen divided by ϕ versus SBE 43 output voltage for the 59.5 section. Oxygen data collected at the East Greenland shelf is not well fitted (blue dots).

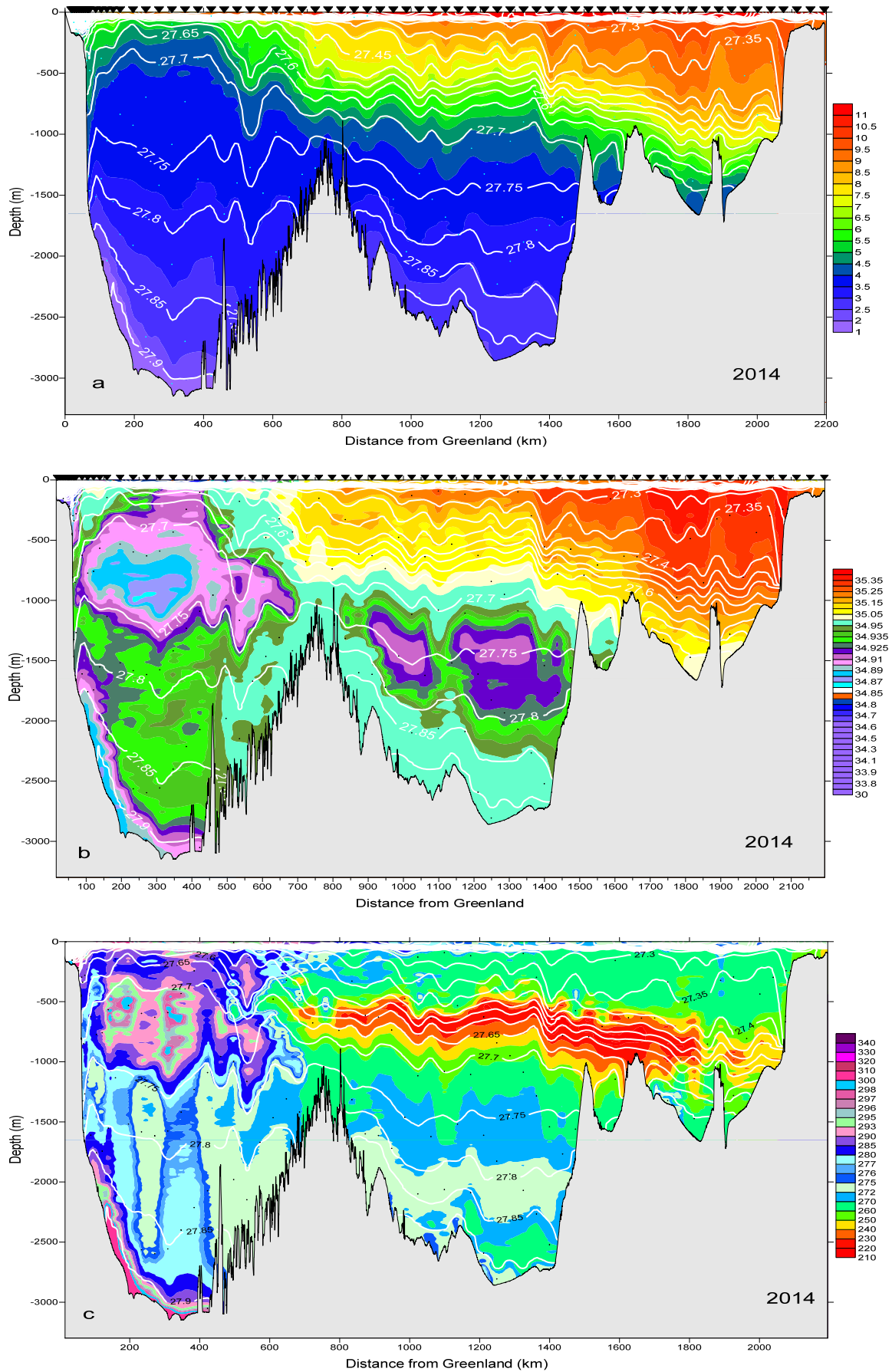


Figure 12 The vertical distribution of (a) potential temperature ($^{\circ}\text{C}$) and (b) salinity and (c) CTD dissolved oxygen ($\mu\text{mol/kg}$) along 59.5 N in 4-15 July 2014. Density is shown in white. Station position is shown by triangles.